MEASURING SHORT-TERM COASTLINE CHANGES FROM AN ACTIVE VOLCANO (AMBAE, VANUATU)

A thesis presented in partial fulfilment of the requirements for the degree of

Master of Science

in

Earth Science

At Massey University, Palmerston North, New Zealand.

Hannah Reid

2021

ABSTRACT

Ambae is a small island in Vanuatu which in recent times has seen high levels of volcanic activity. Between August 2017 and December 2018, several volcanic eruptions occurred, some larger than others, but all with varying effects. A major eruption occurred in July 2018, causing sediment build-up at different locations along the western coastline of the island. The sediment build-up appeared to increase over months, and receded over continuing months.

Analyses were completed to assess and evaluate satellite platforms and their ability to aid in gaining an understanding of coastal change over the time period between August 2017 and December 2018. Imagery from each platform was combined with the use of various water indices which aided in measuring the magnitude of coastal change over the time period.

Sentinel-2, Landsat 8 and Planet satellite platforms were analysed for their effectiveness when used in conjunction with water indices, including the Normalised Difference Water Index (NDWI), Modified Normalised Difference Water Index (MNDWI), and Automated Water Index (AWEI).

The Sentinel-2 platform with the NDWI water index was found to be the most effective for analysing the coastal change. The combination of this satellite platform with this index enabled a quantitative measurement of land change over a specific period of time (August 2017 to December 2018).

ACKNOWLEDGEMENTS

I would like to sincerely thank my supervisors, Associate Professor Jon Procter and Dr. Stuart Mead for their guidance throughout this project. I am grateful for your patience and encouragement, and for showing me so much kindness. Thank you to Jon for always checking in to see how I was going. Stuart, thank you for keeping me on track, for answering all my questions, and for giving me so much of your time.

I am greatly appreciative to the School of Agriculture and Environment at Massey University for their financial assistance as part of the MBIE Endeavour Fund research project “He Tatai Whenua.”

Thank you to my family and friends for your love, support, and advice. I appreciate you all for taking an interest in my studies. A special thank you to my mum and my sister for always trying to help me whenever I needed it, for making me laugh with funny animal videos, and for telling me which sentence sounded the best.

Finally, thank you to Messiah for being there for me throughout this journey I’ve taken. Thanks for your encouragement, for listening, and for always understanding. I appreciate you allowing me to discuss my project with you even when you didn’t really know what I was talking about. Thank you for always pushing me to do my best.

TABLE OF CONTENTS

LIST OF FIGURES

LIST OF TABLES

ABBREVIATIONS

Abbreviation	*Meaning*
ACM	Active connection matrix
AMERL	Automated method for extracting rivers and lakes
API	Application programming interface
ASTER	Advanced Spaceborne Thermal Emission and Reflection Radiometer
AWEI	Automated water extraction index
CSV	Comma-separated values
ESA	European Space Agency
ETM+	Enhanced Thematic Mapper Plus
GIS	Geographic Information System
MIR	Middle-infrared
MNDWI	Modified Normalised Difference Water Index
MODIS	Moderate Resolution Imaging Spectroradiometer
MSS	Multispectral Scanner System
NDVI	Normalised Difference Vegetation Index
NDWI	Normalised Difference Water Index
NDWI_PCs	Normalised Difference Water Index Principle Components
NIR	Near-infrared
NNDiffuse	Nearest neighbour diffusion
OLI	Operational Land Imager
PAN	Panchromatic
PCA	Principle components analysis
RADAR	Radio Detection and Ranging
REMAP	Remote ecosystem monitoring and assessment pipeline
RGB	Red green blue
SAR	Synthetic Aperture RADAR
SNAP	Sentinel Application Platform
SPOT	Satellite Pour l'Observation de la Terre (Satellite for observation of Earth)
SWIR	Short-wave infrared
TM	Thematic mapper
TIRS	Thermal Infrared Sensor
UDM	Unusable data mask
USGS	United States Geological Survey
VNIR	Visible near-infrared
WRI	Water Ratio Index
WV-WI	WorldView Water Index

1 INTRODUCTION

The coastline is the meeting point of the land and sea. It is an environment with constant changes due to the shifting of waves and sea-level, and variations in the supply and movement of sediment from land (Bryan et al., 2008). New Zealand is a country of islands in a highly tectonically active, volcanic environment which is susceptible to frequent coastal change. The impact of coastal sedimentation processes, including coastal erosion, could have negative physical implications enhancing sea-level rise, a greater prevalence of adverse weather conditions, and coastal flooding (Gallina et al., 2019). The negative implications of coastal erosion would also have an effect on coastal sedimentation, particularly with an increase in storm surges as this is the primary agent in coastal sediment transport (Davidson-Arnott, 2009). In New Zealand it is important to explore to understand how this sort of process would affect the environment in a short timeframe. This understanding could be used for coastal development planning, hazard zonation, and for the prediction of coastal change with future events (Maiti et al., 2007).

Deposition, or sedimentation is a geological process where material is added to a landform (Jones, 2008) and "coastal sedimentation processes" refers to any force or activity which impacts the sediment along a coastline, whether this is the deposition, transportation or erosion of the sediment (Horikawa, 1981). Coastlines change often, and this change can occur quickly or over a long time. In the short term, change can occur due to high energy events such as storms and cyclones (Robertson et al., 2007). Usually, shoreline change from such events is caused by high wave action initiated by strong winds from the storms. These events are also often cyclical, occurring more frequently at certain times of the year when the weather is harsher and winds of certain directions are stronger, causing greater wave action and damage to the coastline (Ryabchuk, 2012).

Short-term coastal change can act as an enabler for medium to long-term coastal change where an increased frequency of high energy events over a short time leads to longer-lasting change (Bryan et al., 2008). In cases like this, storm events may occur frequently

over one year, but the coastline may take several years to completely recover (Bryan et al., 2008). Coastal change at the medium to decadal scale can also be cyclic, where there are natural periods of coastal erosion followed by periods of progradation or sediment growth, however, these periods can also be influenced by external factors such as sea level and wave changes caused by climatic shifts, or due to a sea level rise (Bryan et al., 2008).

These studies mostly consider how coastal sediment processes may affect the existing coastal sedimentation, but there are few studies (e.g. Jones, 2008) which explore the possible changes of coastal sedimentation caused by changes to the supply of the sediment. Sediment supply can be long-term, where suspended sediment within rivers naturally flows to the coast and can be easily measured (Hicks et al., 2011) but short-term 'shocks' to supply are also important (Robinson et al., 2013). Events such as earthquakes, volcanic eruptions, or large landslides have the potential to significantly impact the sediment supply in an area, but the magnitude of change cannot be definitively measured without such an event occurring. It is, however, possible to predict the potential consequences from such events, which is important to do to understand how the landscape could change and in what ways (Robinson et al., 2013).

Field surveys and aerial mapping provide a way to identify coastal changes over a small area in an effective and precise way, but often come at high cost. On the contrary, satellite remote sensing offers a way of gathering the same information at a larger scale and at a low (often free) cost (e.g. Guariglia et al, 2006). With satellite technologies advancing, the spatial and temporal resolutions mean that satellite remote sensing is now a reliable way to investigate and monitor coastline change. Previously, identifying short-term coastal change using satellite remote sensing has been difficult due to low temporal resolution (revisit time) of certain areas and poor-quality images due to low spatial resolution (Cao et al., 2019). With new technologies and an increased demand for satellite remote sensing, these are no longer issues. Satellite-captured imagery is widely-available at high temporal and spatial resolutions. For this, reason, it is now possible to identify short-term changes in coastline using satellite imagery.

There are many satellite platforms and methods available for mapping coastline changes, but the most commonly used satellite platform for this is Landsat, including Thematic

Mapper (TM), Enhanced Thematic Mapper (ETM+), Multispectral Scanner (MSS), and Operational Land Imager (OLI). Most of these studies focus on coastal change that has occurred as a resultof human activity or from natural causes like wave energy, sea level, or sediment supply (Kourosh Niya et al., 2013), but they have not been evaluated for their ability to identifyshort term 'shocks' in sediment supply.

Through a case study at Ambae Island, Vanuatu, this study evaluates available techniques and satellite platforms to examine coastline changes caused by short term shocks in sediment supply. The use of remote sensing imagery to identify and measure changes in sediment supply over a short time that has resulted from a volcanic eruption is important as it is something that has occurred in New Zealand (Manville et al., 2005) and could occur again. The similar setting of a volcanic shock in sediment supply between Ambae and the New Zealand landscape means this case study can be used as an effective comparison for the impacts such an event could have.

1.1 Aims and Research Objectives

The aim of this thesis is to assess and evaluate satellite platforms and their ability to aid in gaining an understanding of coastal change over a ~one-year time period due to short-term 'shocks' in sediment supply.. The satellite platforms will be assessed based on their effectiveness in displaying imagery of interest, as well as how they work when used to detect the coastal changes. The most important aspect of this will be the satellite platforms' ability to allow for accurate measurement of the magnitude of change along the coastline due to increased sediment load produced by volcanic eruptions across the one-year period. It will also be important that the resulting data is easily interpreted and provides a clear and definitive analysis of the coastal change.

To achieve this, the thesis has the following objectives:

1. Collect and study multiple satellite imagery datasets and prepare them appropriately to be used for analyses
2. Using each dataset, create a timeline to show predominately cloud-free areas over the course of the eruptions
3. Find areas of interest (areas where coastal sediment has built up the most) within the cloud-free areas and conclude which dataset is the best to use
4. Determine which water index will be the most effective to differentiate between water and sediment by testing each one (NDWI, MNDWI, AMERL, AWEI) on the chosen dataset
5. Complete a change detection analysis to measure how and where the sedimentation has changed over time
6. Determine the relationship between the sedimentation and the volcanic activity and what effects future eruptions may have on the island

Following these aims and objectives during the entirety of this study will help to effectively analyse the volcanic sedimentation on Ambae's coast in a way that is relative to New Zealand's environment. There are certain aspects of the aims and objectives where specificity is imperative. For example, the need to select cloud-free data is essential for making the processes within the analyses simpler and less time-consuming. To organise the cloud-free images across the desired timeframe is also important to ensure that adequate imagery has been obtained. The image acquisition dates across the timeframe must be variable enough so that significant changes in the environment can be identified. Lastly, the water indices listed in the Objectives section have been chosen based on their use in previous, similar studies to this one. It is still unknown whether the indices will be effective to complete what is desired in this study which is why they must all be tested.

1.2 Thesis Structure

Chapter 1: Introduction

Chapter one contains an introduction to coastline and the sediment processes which occur there. It also contains an introduction as to how satellites and satellite imagery can be used to capture the processes that occur at the coastline. As well as this, it contains the aims and objectives of this thesis, and an introduction to the study area and the volcanic eruptions that occurred on Ambae.

Chapter 2: Literature review

Chapter two contains an introduction to remote sensing, the different types of sensors and satellites available. It also contains a review of the potential remote sensing methods and processes that could be used during this study.

Chapter 3: Data review

Chapter three contains a review on the potential satellite image datasets which could be used for this study. It also discusses the suitability of each dataset with regard to the potential methods and processes, which is determined based on the ease of use of the data, and the specifications required for the remote sensing methods to be used.

Chapter 4: Methods

Chapter four describes how all aspects of this study were completed, including data collection, image processing, water index calculations, and further image analysis. The chapter provides the information necessary to understand how the results were found and the methods that were taken to reach those results.

Chapter 5: Results

Chapter five contains the results from the completed methods which includes a visual comparison of the water indices as well as a visual timeline to show the coastal changes which occurred at Ambae due to the volcanic eruptions before, during and after this time period. The chapter also contains graphs which were created using the data from the water index images to statistically display the coastline changes over time.

Chapter 6: Discussion

Chapter six contains a discussion of the image platforms that were used including a comparison of each one to determine which was the most effective for this study. It also compares the water indices that were used, with a discussion of how each one performed, and ultimately which one provided the best results.

Chapter 7: Conclusion

Chapter seven contains a summary of the overall thesis, and links back to the aims and objectives which were discussed during this introduction.

1.3 Study Area

The island of Ambae, located at approximately 15.389°S latitude and 167.835°E longitude, is the largest of 83 islands and islets in Vanuatu (Bani et al., 2009), (Figure 1 below). It is the emergent part of the largest volume volcano in Vanuatu, Manaro Voui, which is a shield volcano (Cronin et al., 2004). The island itself is only around 400 km^2 and sits at an elevation of 1,496 m at the summit (Cronin et al., 2004). There are two major crater lakes at the summit, Manaro (50 million m^3 water) and Vui (11 million m^3 water), which contain a variety of volcanic gases (Cronin et al., 2004).

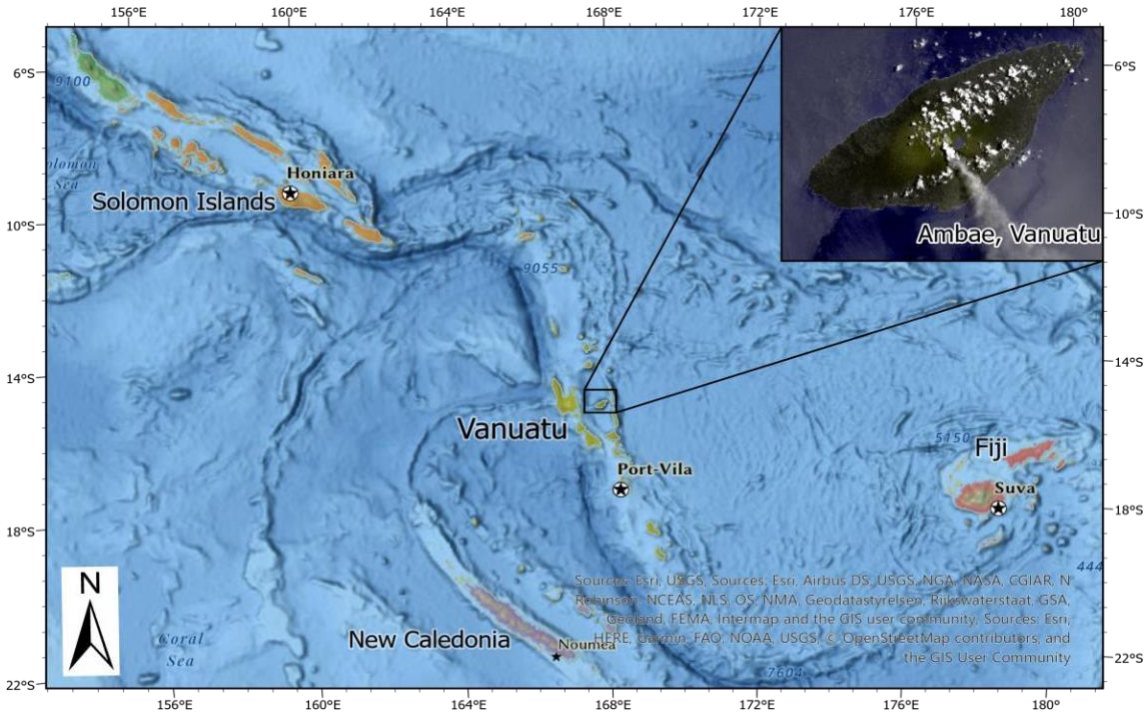

FIGURE 1 THE GEOGRAPHICAL LOCATION OF AMBAE, VANUATU AND SURROUNDING ISLAND NATIONS

Much like New Zealand, Ambae is a region with high levels of tectonic activity. As well as this, the weather patterns across Ambae are like New Zealand. For example, the area is often under cloud cover, particularly over the volcano itself. Due to these factors, Ambae is highly comparable to New Zealand, and so situations in which remote sensing is used could also be applied to situations in New Zealand. An example of this is the ability to retrieve cloud-free remotely sensed images – often it can be difficult to find images of specific locations that are free of or low in cloud. For this reason, methods and ideas used during this project could be used in similar ways in a New Zealand application.

1.3.1 Timeline of eruption events on Ambae

The period of eruptive activity on Ambae, Vanuatu began in September 2017 and lasted for approximately one year. The eruptive activity increased and decreased in intensity at various times throughout this time period, with the most intense eruptive episode occurring during July and August of 2018.

The timeline below highlights the most significant events that occurred during the one-year time period.

September 2017 – In early September the potential for eruptive activity began to increase due to the changing conditions at Aoba. The alert level was raised to 3 (out of 5) on September 6 which signified the volcano was in a minor eruptive phase. The volcanic activity continued to increase, and the alert level was raised to 4 on September 23. Between September 24 and October 5, ash plumes and lava fountains were observed rising from the vent (Global Volcanism Program, 2017).

October 2017 – On October 6, the alert level was decreased to 3 as there was no evidence of the eruption escalating. However, ash plumes of up to 3.7 km above sea level were observed via satellite imagery during October 10-11. Throughout the month of October, ash plumes continued to be observed via satellite imagery on various dates, some of which reached heights of approximately 9 km above sea level (Global Volcanism Program, 2017).

November 2017 – Ash plumes from the volcano continued to be observed across the month of November, however these were much lower, only reaching approximately 3.7 km above sea level at maximum. By the end of November, the eruptive activity had decreased even further, so the alert level was lowered to 2 on December 7 (Global Volcanism Program, 2017).

February 2018 – Across the month of February, eruptive activity was again observed, with ash plumes rising up to approximately 5 km above sea level recorded (Global Volcanism Program, 2018).

March 2018 – The eruptive activity continued into March. This activity was similar to what was observed during October 2017, and therefore the alert level was again raised to 3 (Global Volcanism Program, 2018).

April 2018 – The eruptive activity continued throughout April, with ash plumes rising, as well as some lava fountaining. As well as this, ash, scoria, and acid rain fell across the island. Further observations confirmed that the cone of Aoba had grown, and the crater was larger (Global Volcanism Program, 2018).

May 2018 – Eruptive activity began to decrease over this month, and the alert level was lowered to 2. By June, the activity had stopped (Global Volcanism Program, 2018).

July 2018 – Minor eruptive activity was observed at the beginning of July, and intensified throughout the month. By mid-July, the alert level was raised to 3, with eruptive activity becoming even more intense. Ash plumes became more frequent and there was sustained ash cover across the island, causing daylight hours to become dark. Explosions were observed on July 26 and 27, as well as large ash plumes causing heavy ashfall in neighbouring islands. After these events, an island-wide evacuation order was in place (Global Volcanism Program, 2018).

August 2018 – The large ash plumes continued to rise from the crater throughout the month of August, some of which rose approximately 11 km above the crater rim (Global Volcanism Program, 2018).

September 2018 – The eruptive activity began to decrease over this month, and on September 21 the alert level was lowered to 2. From this date, only steam emissions were observed, and the eruption was considered to have ceased (Global Volcanism Program, 2018).

2 REVIEW OF REMOTE SENSING PROCESSES

2.1 Introduction to remote sensing

Remote sensing is the capturing of images of the earth and its environments using remotely managed technologies (Manolakis et al., 2016). This chapter will review existing remote sensing sensors, platforms, processes and methods which can be used to detect coastline changes. One example of remote sensing is using satellites to capture the imagery. The satellite platforms and the sensors onboard those will be the main focus in this review.

Remote sensing is useful because it allows us to see and gather information on areas of the world that cannot be easily accessed. Sensors on-board the satellites capture images by measuring reflectance of electromagnetic energy. There are different sensors which measure this energy at different wavelengths, resulting in different images. The sensors can also be active or passive, which will again impact the resulting image.

2.1.1 Active vs. passive sensors

In remote sensing, the system used is either active or passive. An active sensor is one which emits its own energy source towards a target and measures the energy that is reflected back from that object (Manolakis et al., 2016). Because an active sensor produces its own energy source, images can be taken day or night. An example of an active sensor is radar. A passive system does not have its own energy source, instead, it measures naturally occuring radiation that has been reflected (e.g. light from the sun) or emitted (e.g. heat) from its source (Manolakis et al., 2016). This study will focus on passive sensors.

2.2 Remote Sensing Sensors

2.2.2 Multispectral sensors

An important aspect of multispectral sensors is their ability to sample the electromagnetic spectrum measuring a larger range of electromagnetic radiation, or light. The spectrum ranges from radio waves to gamma rays, however the most important section in remote sensing is that of the infrared – UV zone (Manolakis et al., 2016). A multispectral sensor can detect radiation within the entirety of this zone, which is why there are various imagery types available.

2.2.3 Visible light sensors

Within a multispectral sensor there are bands that detect light within the visible part of the electromagnetic spectrum (Manolakis et al., 2016). This visible light is seen as the red, blue and green bands.

2.2.4 Thermal Infrared sensors

Most multispectral sensors collect data from the visible and near-infrared spectrum as well as the thermal-infrared. However, there are also some satellites which have a separate sensor measuring the thermal-infrared spectrum only, such as Landsat-8's thermal infrared sensor (TIRS) (Kuenzer & Dech, 2013). The Advanced Spaceborne Thermal Emission and Reflection Radiometer (ASTER) sensor on-board the Terra satellite also collects thermal infrared data. Thermal infrared sensors detect radiant energy which is emitted from earth and can be used to measure relative surface temperatures (Kuenzer & Dech, 2013). It can be difficult to measure surface temperatures over land, but over water it is much easier as there is a known emissivity.

Most multispectral sensors are passive systems, so they will only measure the reflectance of the surface below them and for this reason, imagery can be negatively affected by atmospheric conditions such as clouds.

There are various multispectral sensors which can and have been used for a variety of tasks in different industries, with certain bands being of greater importance to particular

tasks and industries. For example, wavelengths in the near-infrared portion of the spectrum strongly reflect vegetation so are useful in industries such as forestry and agriculture. The wavelength of water emissivity = 0.98 µm, and of healthy plant leaves emissivity = 0.96 – 0.99 µm (Kuenzer & Dech, 2013) which is why differences can be recognised through satellite imagery.

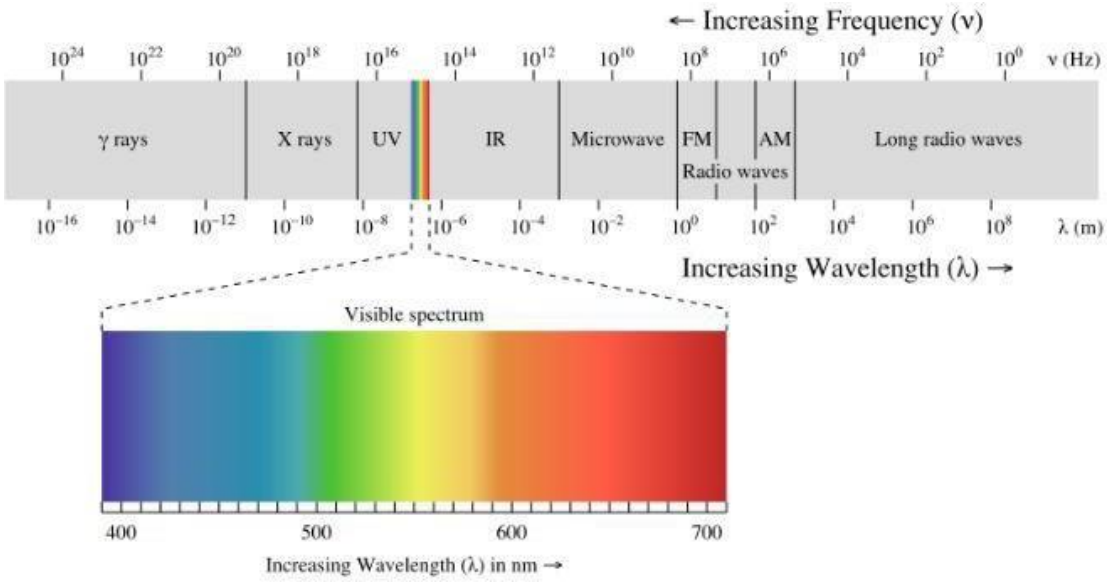

FIGURE 2: THE ELECTROMAGNETIC SPECTRUM HELPS TO VISUALLY UNDERSTAND THE TYPES OF WAVES THAT ARE USED BY MULTISPECTRAL SENSORS, AND WHERE THE WAVELENGTHS SIT ON THE SPECTRUM. FROM: KHAN ACADEMY

Landsat-8 and Sentinel-2 multispectral imagery can be used in various ways, including tasks involving vegetation, but also for the mapping of water bodies and detection of coastlines. These such tasks have been previously completed in various studies (e.g. Du et al., 2016; Rokni et al., 2014); however, it is Landsat imagery that has most often been used.

2.2.5 RADAR sensors

It is significant that SAR imagery can be used for extraction of coastline and change detection, because this makes it an important prospective data type since it also is not affected by cloud.

Radar, in particular synthetic aperture radar (SAR) is an example of an active sensor. The sensor sends microwave (radio) signals downward and detects the backscatter waves that are reflected back to it from objects on the ground (Meyer, 2019). Sentinel-1a and 1b are satellites which both have SAR instruments on-board. Being an active system, SAR is useful because it has the ability to operate day or night as it is not reliant on sunlight (Meyer, 2019). Because the wavelength of SAR is longer than other sensors (for example, SAR is between 1mm and 1cm, all others are below 1mm), it is not susceptible to atmospheric scattering like shortwave sensors (Meyer, 2019). This gives SAR the ability to penetrate through clouds and almost any weather condition except for heavy rainfall (Meyer, 2019).

SAR imagery has been used for the delineation of water bodies or water extent, as well as processes involving change detection of land over time. Huang et al. (2018) developed an algorithm which can be used to automatically extract the extent of the surface water of small water bodies in North America. Their methods involved using Sentinel-1 data to identify the extent of wetlands and distinguish between water and non-water areas.

2.3 Water indices

The literature which describes the development of methods to extract water features using water indices (for example, Normalised Difference Water Index, Modified Normalised Difference Water Index, Automated Water Extraction Index, and the Automated Method for Extracting Rivers and Lakes) have all been completed using Landsat imagery, but this is not to say they cannot be used with another satellite platform. The use of water indices will support the identification of features of interest (e.g. water, land, vegetation) through relative measures of reflectance at specific wavelengths. Most images separate these wavelengths into 'bands' representing the main emission (e.g. 'red' bands typically around 650 nm).

The Normalised Difference Water Index (NDWI) was developed by McFeeters (1996) to help with delineation of open water features. The method uses reflected near-infrared

radiation as it is readily absorbed by water (so will have a lower reflectance on the sensor) and reflected by vegetation and dry soil (so will have a higher reflectance on the sensor) just as readily (McFeeters, 1996). However, there are some limitations with this method. The NDWI works well when only water and vegetation are involved, but not as well in urban areas, which can act similarly to areas along coastlines where there is bare land with high reflection. To combat this issue, Xu et al. (2006) developed a modification of the normalised difference water index (MNDWI). This method also used Landsat imagery, however, middle infrared radiation (MIR) was used in place of near infrared radiation (NIR). The reason MIR was used instead of NIR is because water absorbs more MIR light than NIR so the water will have greater positive values than those of the NDWI. As well as this, areas of built up land will have negative values compared to the NDWI where this type of land was often mixed up with water. Vegetation will also still have negative values.

Like both the NDWI and MNDWI methods, the Automated Water Extraction Index (AWEI) developed by Feyisa et al. in 2013. Again, using Landsat data, their idea was to increase the contrast between water and non-water surfaces in order to maximise their separation.

The automated method for extracting rivers and lakes from Landsat imagery (AMERL) was created by Jiang et al. (2014). Although the focus was on small water bodies, it would be possible to apply this method to larger water features such as a sea or ocean. The AMERL is different to the methods previously mentioned as it can be used to identify mixed water pixels which often occur in shallow or narrow water bodies (Jiang et al., 2014).

These examples (NDWI, MNDWI, AMERL) all used Landsat sensor platforms, however could be used with other platforms (e.g. Sentinel-2, Du et al., 2016) or with multispectral sensors. Using Sentinel-2 imagery, Du et al. (2016) applied the MNDWI method by pan-sharpening the short-wave infrared (SWIR) and visible and near-infrared (VNIR) bands to match the resolution of the visible bands. Pan-sharpening of these bands has been completed in the past using various methods, Park et al. (2017) most recently.

2.3.1 NDWI

The normalised difference water index (NDWI) is an equation which is calculated on a satellite image to try to delineate open water features of the image. It is based on similar ideas as the NDVI, which aims to highlight vegetated areas of an image, but by reversing the NDVI equation, open water features can instead be highlighted.
The NDWI equation is as follows:

$$NDWI = \frac{Green - NIR}{Green + NIR}$$

The near infrared band is used because water strongly absorbs NIR and vegetation strongly reflects NIR. The green band is used because it holds reflected green light, and these green wavelengths are able to maximise the reflectance of water. Overall, the equation will 1) maximise the typical reflectance of water features by using green light wavelengths, 2) minimise the low reflectance of NIR by water features, and 3) take advantage of the high reflectance of NIR by terrestrial vegetation and soil features (Xu, 2006). Once an image has been processed with the equation, water features will have positive values while soil and terrestrial vegetation features will have zero or negative values.

2.3.1 MNDWI

The modification of normalised difference water index (MNDWI) was created as the NDWI cannot effectively distinguish between built-up land noise and extracted water features which causes them to become mixed up (Xu, 2006) which could be an issue when measuring coastline changes. The pixels become mixed because the green band and the NIR band have a similar reflectance pattern for built-up land and water, where they both reflect green light more than they reflect infrared light (Xu, 2006). Thisresults in positive values for both water and built-up land.

The MNDWI equation is as follows:

$$MNDWI = \frac{(Green - MIR)}{(Green + MIR)}$$

The equation shows that the middle-infrared band is used in place of the near-infrared band. By using the MIR band, the built-up land areas should have negative values instead of positive. This is because the average digital number of the MIR band is much greater than that of the green band. When the MNDWI is computed, it should result in: 1) water having greater positive values than in the NDWI as it absorbs more MIR light than NIR light; 2) built-up land having negative values, and 3) soil and vegetation also having negative values as soil reflects MIR light more than NIR light and vegetation reflects MIR light more than green light (Xu, 2006). These factors should result in there being greater contrast between the water features and the built-up land features.

2.3.2 AWEI

The Automated Water Extraction Index (AWEI) was created to try and improve the accuracy of surface water mapping by automatically suppressing classification noise from shadow and other non-water dark surfaces such as asphalt or dark coloured rooves (Feyisa et al., 2014). As well as this, it aims to show effectively this new method would work under different environmental conditions and to compare it against existing methods. When the AWEI was created, the images used were of various water bodies in different areas and conditions from five different countries. The range of test sites broaden the applicability of this equation to work with accuracy no matter what the conditions of the image were like. To maximise the separability of water and non-water pixels, band differencing, addition, and the application of different coefficients were used (Feyisa et al., 2014). This has resulted in the creation of two separate equations to ensure maximum effectiveness. The two AWEI equations are as follows:

$$AWEInsh = 4 \times (\rho green - \rho SWIR1) - (0.25 \times \rho NIR + 2.75 \times \rho SWIR2)$$

$$AWEIsh = \rho blue + 2.5 \times \rho green - 1.5 \times (\rho NIR + \rho SWIR1) - 0.25 \times \rho SWIR2$$

The coefficients used in the equations and the combinations of the bands were chosen based on the reflectance properties of different land cover types. Particular importance

was placed on the need to enhance the separability of water and dark surfaces such as shadow and built-up areas as they are often difficult to distinguish as they have similar reflectance patterns. The coefficients were also chosen so that non-water pixels would be forced below zero, and water pixels above zero in order to increase the stability of the equations (Feyisa et al., 2014).

The $AWEI_{nsh}$ equation should effectively eliminate non-water pixels, including dark built surfaces in areas with urban background and is best used for areas without shadow. The $AWEI_{sh}$ helps to improve accuracy by removing shadow pixels that $AWEI_{nsh}$ may not be able to, so is best used for areas with shadow and/or other dark surfaces as it could misclassify water surfaces where there are other highly reflective surfaces such as snow, ice, and reflective roof tops in urban areas. In terms of coastline change, the $AWEI_{nsh}$ is likely to be useful for analysing coastline change as there would not usually be any features that are likely to cause shadow, like large buildings. The $AWEI_{sh}$ could be useful for analysing coastline change in areas where the coast is next to highly forested areas.

2.3.3 AMERL

The automated method for extracting rivers and lakes (AMERL) was developed by combining water indices with digital image processing techniques to identify water pixels, particularly mixed water pixels in shallow or narrow water bodies (Jiang et al., 2014). The aim of the AMERL was to properly identify mixed water pixels and to capture the mixed water pixels with minimal noise; two issues which often occur when using water indices.

To achieve the AMERL, pure water pixels were extracted using a deliberately selected strict threshold (Thd_{pure}) (Jiang et al., 2014). They tested Thd_{pure} for each WI (NDWI, MNDWI, $AWEI_{sh}$, and $AWEI_{nsh}$) using a number of training images with stable characteristics (Jiang et al., 2014). Next, a watershed segmentation method was used to identify mixed water pixels at the edges of lakes or wide rivers (Jiang et al., 2014). Then, a method based on linear feature enhancement was used to identify water pixels from narrow rivers (Jiang et al., 2014). Lastly, the extracted water features were combined to produce a final water body (Jiang et al., 2014).

2.4 Remote sensing processes

2.4.1 Extraction of coastline/water bodies

There is no single method to be used for shoreline modelling or coastline extraction, however, the use of remote sensing has become one of the most effective ways to do so (Dominici et al., 2019). By using remote sensing for this type of process, various methods can be explored to determine which of these are appropriate in situations where the coastal change is caused by a natural disaster.

Satellite imagery from WorldView-2 has previously been used in studies where it was necessary to identify or extract the coastline. In one study, this was completed using NDVI and NDWI water indices to classify images to show sea, land, and vegetation (Maglione et al., 2014). Normally, NDVI is used to estimate vegetation density, but it is also able to distinguish between water and bare soil (Maglione at al., 2014), which is why it was used in this case. After calculating the NDVI and NDWI for the images, a Maximum Likelihood criterion was applied to find the threshold values for each index (Maglione et al., 2014) and the resulting images were vectorised to show the three classes only. By comparing the vector images with pan-sharpened RGB (regular coloured) images of the same locations, it was possible to see which index was able to most effectively identify the coastline (Maglione et al., 2014).

WorldView-2 imagery was also used to extract the shoreline using New Enhancement Algorithms (Dominici et al., 2019). The Coastal Band available with WorldView-2 imagery makes the use of the NDWI equation more effective at differentiating between water and land due to the large difference between the Coastal Band and the NIR band (Dominici et al., 2019). A classification process is often used in conjunction with equations such as NDWI, however it can be difficult to decide on the number of classes to use, and what type of classes these should be (Dominici, 2019). For this reason, a new method for shoreline extraction was developed which involves the comparison of Active Connection Matrix (ACM) filters (Dominici et al., 2019). First, the images in use had common filters applied to them to find the most effective ones for showing a clearly defined shoreline. These filters included a Principle Components Analysis (PCA), Normalised Difference Vegetation Index (NDVI), WorldView Water Index (WV-WI), and

Unsupervised and Supervised Classifications. It was found that the WorldView Water-Index (WV-WI), which uses WorldView-2 bands to highlight areas of standing water greater than one pixel in size, was the most effective of these methods at defining the shoreline (Dominici et al., 2019).

The ACM system was next used in the processing of the images which involved testing some experimental algorithms to determine their effectiveness for the study (Dominici et al., 2019). In the ACM system, an image is considered to be a network that changes over time where the pixels are the connected elements within the network (Dominici et al., 2019). In other words, the pixels act as a neighbourhood, whereby if one pixel contains the value equal to "vegetation" the surrounding pixels can be compared to that one to find the likelihood that they are also "vegetation."

WorldView-2 imagery was also used in a study (Jawak & Luis, 2015) that was looking to find a way to semi- automatically extract water features in harsh environments that are difficult to access. It is recognised that water indices such as NDWI are commonly used for feature extraction and shoreline delineation (Jawak & Luis, 2015). The use of such a process is unlikely to be effective in Antarctic conditions due to the frozen environment potentially having similar spectrum characteristics as diverse ground targets that would ordinarily be differentiated in indices such as NDWI (Jawak & Luis, 2015). In this study, a new NDWI model was designed to extract water features using pixel-wise methods (Jawak & Luis, 2015). The new NDWI method was also compared against supervised feature extraction algorithms using visual and statistical accuracy (Jawak & Luis, 2015). A PAN-sharpened multispectral image was used to process 14 semi-automatic feature extraction methods which were categorised as either: a) Modified NDWI methods, b) Spectral matching methods, or c) Target extraction methods (Jawak & Luis, 2015). Visual inspection was used to find the best spectral bands for differentiating water bodies, and these were used to create the modified NDWI (Jawak & Luis, 2015). Manual thresholding was used on images with areas where meltwater on the snow surfaces could have been confused for water bodies (Jawak & Luis, 2015). Each image was then classified using the modified NDWI to extract the 36 water bodies, and these were then vectorised so that the area of each one could be calculated (Jawak & Luis, 2015).

Multitemporal Landsat ETM+, TM, and OLI imagery was used in a study (Rokni et al., 2014) which aimed to find an effective technique for measuring surface water changes at Lake Urmia in Iran between 2000-2013. This study recognised that there have been several image processing techniques introduced in recent times, but many of them are single-band methods that make use of a selected threshold value to extract water features. Such a processing method can have errors, as water pixels can often be mixed with pixels of other cover types (Rokni et al., 2014). The use of multi-band methods can improve surface water extraction, for example, NDWI, MNDWI etc.

For the Lake Urmia study, a new technique to measure surface water change was developed, based on Principal Components of multi-temporal NDWI (NDWI-PCS) (Rokni et al., 2014). The NDWI-PCS method itself was first tested for water-extraction suitability, but as it is usually used for forest-fire detection, it was unsuitable (Rokni et al., 2014). NDWI, MNDWI, WRI, NDVI, and AWEI were also all tested for suitability, and accuracy assessment showed NDWI to be the most effective (Rokni et al., 2014). The Normalised Difference Moisture Index (NDMI), which is normally used to measure the water content of vegetation (Rokni et al., 2014) was then reformulated for surface water extraction by substituting it with NDWI (Rokni et al., 2014). From here, the water surface of the lake was individually extracted from each image over the time period to compare the performance of each water index (Rokni et al., 2014). A land-water threshold (determined using trial and error by comparison to reference maps) was then manually applied to each image to classify them to show land and water only (Rokni et al., 2014). The NDWI-PCs was developed because manual thresholding is time consuming. To complete the NDWI-PCs, the NDWI images were first stacked into one composite file, and then the Principal Components Analysis was performed to turn the composite image into a new PCA space (Rokni et al., 2014).

The Planet CubeSat imagery has also been used for a study (Cooley et al., 2017) involving the tracking of surface water extent in dynamic, high altitude areas. It was chosen for its high temporal

and high spatial resolution. Often, it is necessary to compromise between these two factors. For example, Landsat, Sentinel-2, and MODIS can and have all been used to track surface water extent and/or changes, but there is a combination of issues with these imagery types involving spatial and temporal resolutions, as well as atmospheric issues such as high cloud cover. For these reasons, none of these satellites are completely reliable for this sort of task. It is necessary to observe areas surface water frequently, particularly where the surface water extent is dynamic and at a high latitude. Often, in areas like this, the water bodies are much smaller, and therefore unvisited and unstudied (Cooley et al., 2017). A variety of factors cause this type of water body to change rapidly, such as melting permafrost, or a shorter duration of snow-cover (Cooley et al., 2017). In this study, the Planet CubeSat imagery was used to track changes in surface water extent in a 625 km^2 area within the Yukon Flats of north Central Alaska (Cooley et al., 2017). A number of steps were taken to classify the images into open water and vegetation/surrounding land. These steps included looking for images with less cloud cover and altering these images so that the cloud cover was masked out.

2.2.2 Landscape change analysis for volcanic events

Torres et al. (2004) used remote sensing data to monitor changes to an alluvial fan that evolved after the eruption of Mount Pinatubo in 1991. The study involved collating 10 years' worth of remote sensing imagery to attempt to understand the erosion and deposition processes of the ignimbrite and lahars in a way so that extensive and difficult field work would not be necessary. The imagery collected was from various satellite platforms due to the different bands available on these platforms. For example, Landsat TM, SPOT, and ASTER can be used to identify areas with and without vegetation using their visible and near-infrared bands, and this can provide information about whether sections of the lahar deposits are older or younger (Torres et al., 2004). RADAR is useful because it can detect variations in surface roughness – these variations can be dependent on the moisture content within the lahar deposit (Torres et al., 2004), so again, the age of the deposits can be compared. The remote sensing observations made were done so by completing analyses such as Principle Components Analysis (PCA) which

can be used to create image difference maps, where changes in the landscape over time are highlighted using different colours.

Wahab et al., (2019) recognises how devastating a volcanic eruption can be to an environment and the importance of the need to monitor volcanic environments due to the level of change that may occur over such short timeframes. This recognition came from the eruption of Mount Agung, Indonesia in 2017, and the changing environment due to the eruption has been the main focus for this study. Wahab et al., (2019) completed supervised classifications of Landsat 8 imagery to identify the current landcover around the volcano and compared this to previous landcover information using web-based GIS application REMAP. The vegetation density around the volcano was also identified using NDVI calculations (Wahab et al., 2019). The results of the study found that there were five main landcover types surrounding the volcano, and there were areas of high, medium and low vegetation density (Wahab et al., 2019). It is thought that the areas with no vegetation density could be indicative of the direction of the eruption flows (Wahab et al., 2019).

Another method of measuring the change in an environment due to volcanic activity is through change detection analysis. Singh (1989) defines change detection as "the process of identifying differences in the state of an object or phenomenon by observing it at different times." In other words, and in terms of remote sensing, it is the use of satellite images of an area over multiple dates in order to measure changes that may have occurred in the area over time. There are many factors which must be considered before undertaking a change detection analysis, such as what specific points in the image are of interest and which points are not of interest. When completing the change detection analysis, it is the change in reflectance values over the time period that will be measured, so it is also important to choose a change detection method that is suitable for the data and task.

3 REVIEW OF SATELLITE PLATFORMS

The data that is chosen for this project will have certain requirements for its use to be worthwhile. Firstly, the spatial resolution needs to be high enough so that small areas on the island of Ambae can be easily seen. Secondly, the data needs to have the correct bands so that it can be processed with the various water indices that are of interest, including NDWI, MNDWI, and $AWEI_{nsh}$ and $AWEI_{sh}$. The bands needed for these indices include blue, green, NIR, MIR, and SWIR. Lastly, the satellite that provides the data needs to have a sufficient return time and low cloud cover to identify the coastal change.

Landsat, Sentinel and Planet satellite platforms were identified as viable options for data provision based on their use in literature, available bands, and return time. The use of multiple platforms will provide a comparison of the spectral resolution, spatial resolution and return time of each respective satellite. Completing analysis with multiple satellites may also help to combat issues which could arise if platforms are inhibited by cloud cover, spatial extent or return times.

3.1 Landsat 8

There have been many similar studies previously completed using Landsat data which suggests it would be a good choice to use for this study. Where “similar studies” are those which involve the extraction of surface water, the use of water indices to measure water bodies in some way, and/or also completing a change detection analysis on these water bodies. In fact, when searching for articles of these similar studies, the majority of them were completed using Landsat data which is perhaps because the data requires the least complicated pre-processing. Some of these studies were mentioned previously in chapter 2, for example, Rokni et al. (2014) used Landsat data to complete a study of water surface change at Lake Urima, Iran using various water indices.

Landsat 8 OLI/TIRS C1 Level-1 data was downloaded from the USGS website EarthExplorer. The downloaded data dates ranged from July 2017 – March 2019 with

varying levels of scene cloud cover, but with medium low levels of cloud cover over the island of Ambae. It was very difficult to find imagery with low scene cloud cover, so often it was more important to find images only without cloud over the areas of interest on the island. The areas of interest on Ambae are very small so Landsat's low spatial resolution of 30 m is not effective at capturing a clear image of these areas. However, Landsat 8 does have a PAN band of 15 m spatial resolution, which – with extra processing – gives the data the potential to be equally as useful as higher resolution imagery. Landsat is also useful as it has a full range of spectral bands (Table 1) needed for the water index processing and these are all at the same resolution so they can be used as they are. As well as this, the Landsat data collected are all uniform in size and shape which makes it easy to alter across each image if needed.

Landsat 8			
Band number	**Central wavelength (nm)**	**Bandwidth (nm)**	**Spatial resolution (m)**
1 Coastal/Aerosol	443	20	30
2 Blue	482.5	65	30
3 Green	562.5	75	30
4 Red	655	50	30
5 Near infrared	865	40	30
6 SWIR	1610	100	30
7 SWIR	2200	200	30
8 Panchromatic	590	180	15
9 Cirrus	1375	30	30

TABLE 1 SPECTRAL RESOLUTION (BANDWIDTH) AND SPATIAL RESOLUTION FOR LANDSAT 8 BANDS

3.2 Sentinel 2

There have been few similar studies completed using Sentinel 2 data which is perhaps because the pre-processing required for the data to be used is somewhat complicated. It is possible to complete some work with minimal pre-processing, however, to use the data further it needs to be pre-processed due to the fact that not all bands are at the same resolution. It is still possible to use Sentinel imagery for studies involving water indices, as shown by Du et al. (2016) who completed a study using water indices and Sentinel-2 imagery to monitor changes of the Venice coastland.

Sentinel-2A and 2B data was downloaded from the ESA Copernicus Open Access Hub. The downloaded data dates ranged from July 2017 – March 2019 with varying levels of scene cloud cover, with medium to low levels of cloud cover over the island of Ambae. It was almost impossible to find any images that were entirely cloud free, so instead images were downloaded that had some cloud, but were cloud-free in the areas of interest on the island. Sentinel-2 has a spatial resolution of 10 m which means it is effective at capturing the areas of interest. Although Sentinel-2 has the full range of bands required for the water index processing (Table 2), they are not all at the same spatial resolution meaning that to use them, extra processing is necessary. Of the bands needed, the red, blue, green and NIR bands have a spatial resolution of 10 m, and the MIR and SWIR bands a spatial resolution of 20 m. Processing could be completed to either downscale the 20 m bands to 10 m, or upscale the 10 m bands to 20 m. It was more beneficial to downscale the 20 m bands to 10 m so that the spatial resolution level was not lost. The processing for this was completed using a plugin in SNAP called Sentinel 2 Super-Resolution which automatically downscales the 20 m bands to 10 m. This processing was highly time-consuming, so it was necessary to select only a small area of the Sentinel image to be processed. Although the imagery required so much pre-processing, the data could be used effectively as all the images were the exact same in size and shape. The uniformity meant that the images could be altered in size very simply and would in the end still display the desired area.

	S2A		S2B		
Band number	**Central wavelength (nm)**	**Bandwidth (nm)**	**Central wavelength (nm)**	**Bandwidth (nm)**	**Spatial resolution (m)**
1 Coastal aerosol	442.7	21	442.2	21	60
2 Blue	492.4	66	492.1	66	10
3 Green	559.8	36	559.0	36	10
4 Red	664.6	31	664.9	31	10
5 Vegetation red edge	704.1	15	703.8	16	20
6 Vegetation red edge	740.5	15	739.1	15	20
7 Vegetation red edge	782.8	20	779.7	20	20
8 NIR	832.8	106	832.9	106	10
8a Narrow NIR	864.7	21	864.0	22	20
9 Water vapour	945.1	20	943.2	21	60
10 SWIR – Cirrus	1373.5	31	1376.9	30	60
11 SWIR	1613.7	91	1610.4	94	20
12 SWIR	2202.4	175	2185.7	185	20

TABLE 2 SPECTRAL RESOLUTION (BANDWIDTH) SPATIAL RESOLUTION FOR SENTINEL-2 BANDS

3.3 Planet

The Planet CubeSat imagery was acquired under a Planet Education and Research licence, and the dates of this data ranged from August 2017 – April 2019. Table 3 describes the specifications of the Planet imagery, including the spatial resolution which ~3 m. This means it can provide a clear and precise image of any area that is captured. Data format and licence restrictions (limiting the area of the imagery) meant the data came in small "pieces" which had to be mosaicked together so that the whole image could be seen and the arrangement of the data within the folders did not allow this to be completed in a batch process so it was very time consuming. Overall, the Planet data was far less user-friendly than the Landsat and Sentinel data – a compromise to be made for its high resolution. As well as this, the Planet data only has four bands – red, green, blue, and NIR which means it is limited in its usage of water index processing and only the NDWI can be calculated. Even so, it will still be useful to compare the NDWI of Planet with both Landsat and Sentinel to see whether the higher resolution affects the visibility of the areas of interest. Another negative aspect for the Planet data is that the images are irregularly shaped. For example, some of the images are just a very small portion of the whole island whereas others nearly captured the entirety of the island. The irregularity of the images made it difficult to use as it greatly limited the number of images that could actually be considered for further analysis. As well as this, it was more difficult to measure cloud pixels.

There are very few similar studies that have been completed using Planet data. This is perhaps because there are few bands associated with the data (red, blue, green and NIR), and it is not possible to complete this type of study without the extra bands needed for the water indices. However, Cooley (2017) did complete a study using Planet CubeSat imagery and water indices to map changes in surface water extent in high altitude areas, which is why it remains as a viable option for this thesis.

Planet			
Band number	**Central wavelength (nm)**	**Bandwidth (nm)**	**Spatial resolution (m)**
1 – Blue	482.5	65	3
2 – Green	555	80	3
3 – Red	650	90	3
4 – Near infrared	820	160	3

TABLE 3 SPECTRAL RESOLUTION (BANDWIDTH) AND SPATIAL RESOLUTION FOR PLANET BANDS

3.4 Summary

There are various considerations to be made in deciding which of the satellite platforms could be the most effective for the analyses to be completed, including return time, spatial resolution and spectral resolution. There were many images provided with the Planet data, which is representative of the quick return time of the satellite (almost daily). However, a significant number of these images were unable to be used as they only covered a small portion of the island or did not contain the areas which were of interest. After sorting through the Planet images, there were 11 images that could be used. There were 16 Sentinel-2 images collected from the ESA website, however only nine could be used for further analyses due to too much cloud cover. There were a high number of Sentinel-2 images available for download due to the relatively fast return time of 2-3 days from Sentinel's two satellites, however many of them were not selected for download if the cloud cover looked to be too high, for example, if the majority of the island was covered in cloud, or if the areas of interest appeared to be covered in cloud. There were 11 landsat 8 images downloaded from EarthExplorer, however only eight of these images could be used for further analyses due to a high level of cloud cover. Landsat had the lowest number of available images for download which is representative of its slower return time of 16 days. This information shows that a quick return time will not necessarily equate to a greater number of useable images.

There are also a few important differences to note between each satellite platform which table 4 can help to explain. Landsat has the lowest spatial resolution for all of its bands across each of the platforms, and it has a mid-range spectral resolution (bandwidth). Sentinel has a good spectral resolution and a reasonable spatial resolution. Planet, meanwhile, has a very high spatial resolution, but the sensors have the largest bandwidths and there are fewer available bands. Although a high spatial resolution may provide more accurate measurement of sedimentation areas, a wide bandwidth may reduce the accuracy of calculated water indices and limit the ability to identify thresholds for land/water.

Band	*Landsat*		*Sentinel*		*Planet*	
	Bandwidth (nm)	**Spatial resolution (m)**	**Bandwidth (nm)**	**Spatial resolution (m)**	**Bandwidth (nm)**	**Spatial resolution (m)**
Blue	65	30	66	10	65	3
Green	75	30	36	10	80	3
NIR	40	30	106	10	160	3
MIR/SWIR	100	30	94	20	N/A	N/A

TABLE 4: A SUMMARY OF THE BANDS THAT ARE NEEDED FOR THE WATER INDICES. EACH INDEX REQUIRES DIFFERENT BANDS, BUT THIS TABLE DISPLAYS ALL BANDS NEEDED ACROSS ALL OF THE INDICES. NOTE: PLANET'S BLUE BAND WAS NOT USED AS THE INDEX FOR WHICH IT WOULD BE USED ALSO REQUIRED THE SWIR BAND WHICH IS UNAVAILABLE FOR THAT PLATFORM.

4 WATER INDEX ANALYSIS AND IMAGE PROCESSING

4.1 Data collection

4.1.1 Sentinel-2 data collection

The sentinel-2 data was downloaded from the European Space Agency Open Hub. This website contains all Sentinel imagery (1, 2A, 2B, 3, 5) and collections include all datasets since each of the satellites first launched. Figures 3.1-3.5 show how the imagery was downloaded from this website.

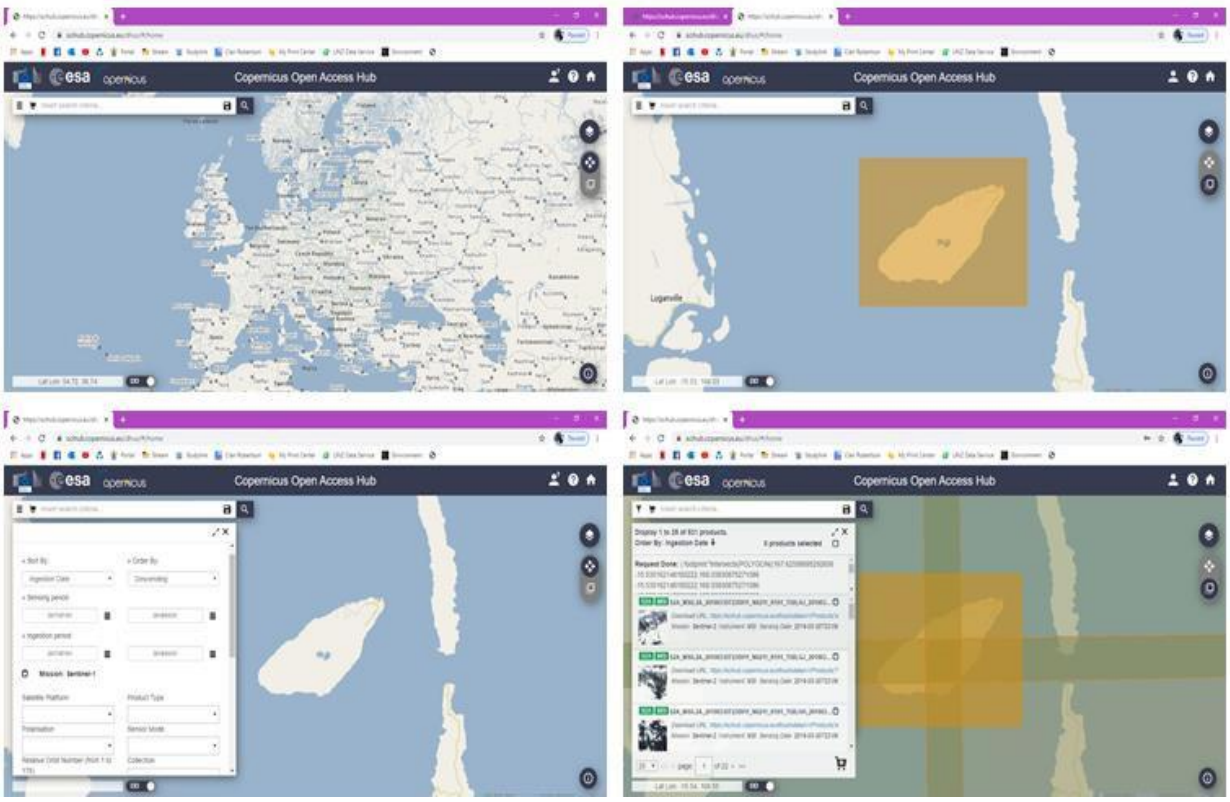

FIGURE 3 THE PROCESS FOR DOWNLOADING SENTINEL-2 IMAGES FOR AMBAE FROM THE ESA OPEN ACCESS HUB.

A) THE HOME PAGE OF THE WEBSITE WHICH CAN BE NAVIGATED BY HOLDING DOWN AND DRAGGING TO THE DESIRED LOCATION; B) AFTER SCROLLING ACROSS THE MAP TO SHOW AMBAE, THE MAP CAN BE SWITCHED TO NAVIGATION MODE BY CLICKING THE PICTURE ON THE RIGHT BELOW THE FOUR ARROWS. ONCE IN NAVIGATION MODE, A BOX CAN BE DRAWN OVER AMBAE TO REDUCE IMAGE RESULTS TO ONLY SHOW ANYTHING WHICH INTERCEPTS WITH THIS BOX; (C) MORE SPECIFIC SEARCH CRITERIA CAN BE ENTERED TO FURTHER REDUCE THE IMAGE; (D) THE RESULTING IMAGES APPEAR IN A LIST SHOWING THE MOST RECENT FIRST.

4.1.2 Landsat-8 data collection

The Landsat-8 data was downloaded from the USGS Earth Explorer website. The imagery is available on other websites, however, Earth Explorer was chosen because is simple to use. This website also has many other satellite datasets available. Figures 4.1-4.4 shows the process for downloading the Landsat-8 imagery.

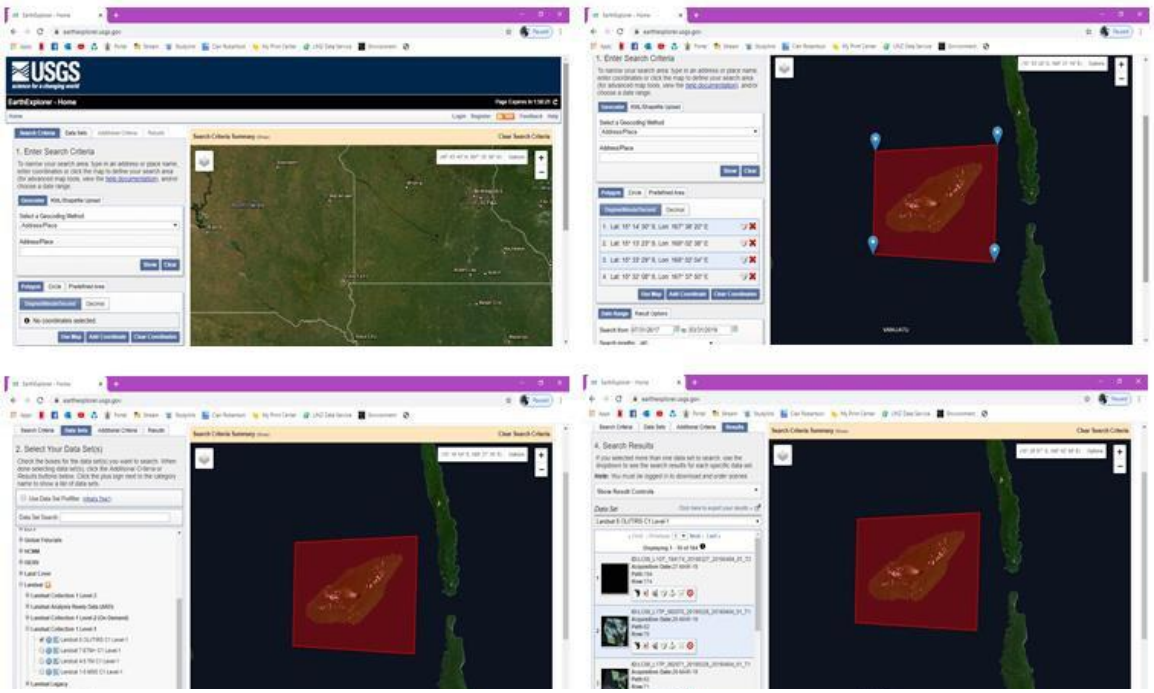

FIGURE 4 THE PROCESS FOR DOWNLOADING LANDSAT 8 IMAGES FOR AMBAE FROM THE USGS EARTHEXPLORER. A) THE HOMEPAGE OF THE WEBSITE PRIOR TO INPUTTING ANY INFORMATION FOR SEARCH REQUIREMENTS IN THE LEFT INFORMATION PANE; B) AFTER NAVIGATING THE MAP TO SHOW AMBAE, A POLYGON WAS CREATED AROUND IT SO THAT ONLY IMAGERY OVERLAPPING THE ISLAND WILL BE SHOWN IN THE RESULTS. THE POLYGON IS CREATED BY SIMPLY CLICKING ON THE SCREEN TO CREATE EACH "PINPOINT" CORNER OF THE POLYGON. THE DATES OF INTEREST WERE ALSO SELECTED SO THAT ONLY IMAGERY TAKEN DURING THE DATES WILL BE SHOWN IN THE RESULTS; C) IN THE NEXT TAB "DATA SETS" THE IMAGERY OF INTEREST WAS SELECTED. IT WAS FOUND BY SELECTING "LANDSAT" THEN "LANDSAT COLLECTION 1 LEVEL 1" AND FINALLY "LANDSAT 8 OLI/TIRS C1 LEVEL-1"; D) THE RESULTING IMAGES FROM THE SEARCH CRITERIA WHICH APPEAR IN A LIST ORDERED FROM LATEST TO EARLIEST. THERE ARE 164 IMAGE RESULTS, HOWEVER IT IS LIKELY THAT MANY OF THESE WILL NOT BE APPROPRIATE FOR USE, THEREFORE IT IS NECESSARY TO PREVIEW POTENTIALLY SUITABLE IMAGES BEFORE DOWNLOADING THEM.

4.1.3 Planet data collection

PlanetScope images were downloaded using the Planet API (https://developers.planet.com/docs/apis/) for a custom-defined region around Ambae shown in figure 5. The region was constrained to a small area due to the Education and Research License for Planet imagery that restricts the maximum area of imagery available. Planet 'Analytic' imagery (radiometric and sensor corrections applied) were downloaded. PlanetScope imagery is derived from the second generation PlanetScope sensors aboard the PlanetScope satellite constellation of ~130 satellites (Planet team, 2017). Data consists of single-frame image 'captures', approximately 24 km × 8 km in size (Planet Team, 2017). The size of these individual images compared to Ambae (~38 km × 16 km) mean a mosaicking step is required to create a composite image from a single date. Each analytical image contains an unusable data mask file (UDM file) that provides information on areas of unusable data (e.g. due to clouds or un-imaged areas). This file was necessary for this study to correctly mask non-imaged areas from calculations.

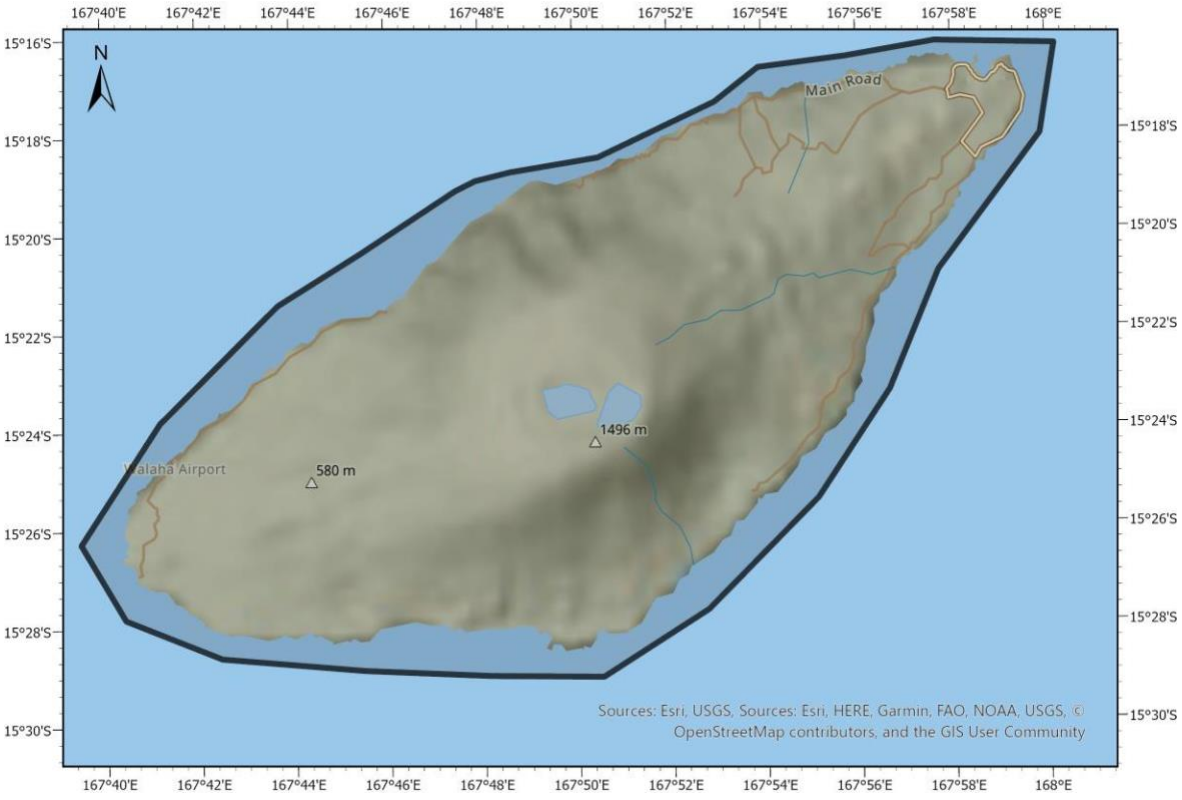

FIGURE 5 THE BLACK OUTLINE IN THIS IMAGE SHOWS THE CUSTOM-DEFINED REGION AROUND AMBAE THAT IS PROVIDED FOR THE PLANETSCOPE IMAGES USING THE PLANET API.

4.2 Image processing

4.2.1 Planet

The Planet imagery was arranged by date in folders each containing a *.tif image and a UDM file for that date. Although they were arranged by date, the imagery could not be used as it was. This was because there were sometimes three or four folders associated with one date. The *.tif images inside the folders were often smaller portions of a larger image all from the same date. Due to this, the imagery had to be mosaicked together so that the full images could be viewed and used more easily. The mosaicking was completed using the Seamless Mosaic tool in ENVI 5.5, and each date was individually selected to ensure accuracy. The mosaicked images were individually inspected for their suitability for further analysis. Any images that were deemed as unsuitable were disregarded; this included images that did not contain a reasonable portion of the entire island, particularly the coastal areas, or images with too much cloud cover, for example, if the majority of the island was covered with cloud or if areas of interest were covered with cloud.

The supplied UDM files could not be easily used as they were in a binary format that could not be read by ArcGIS Pro. For this reason, the files were edited so that they would display as a *.tif image. Once they had been changed to *.tif files, the UDM images were also mosaicked together in the same way as previously described.

Analyses using the mosaicked images and UDM files were for the index images (figures 5-8). Further analysis using histograms (see sections 4.6 and 4.7) required use of a custom histogram toolbox written in ArcPy. In the toolbox, the NDWI value was extracted from each pixel of each image and sorted into 200 bins between -1 and 1 which could be opened in Excel as a CSV file. The toolbox also excluded all cloud pixels from the extracted data. This was completed by including the UDM file as a secondary file for each corresponding NDWI image – the toolbox was able to read both files and only extract the pixel values which did not intersect with the pixels of the UDM file.

4.2.2 Sentinel 2

The Sentinel-2 data required a significant amount of time-consuming pre-processing.

The downloaded Sentinel-2 data for each selected date contained four large tiles – due to the way the imagery was captured by the Satellite, Ambae was in the very centre of these four tiles which is why all four needed to be downloaded. After downloading the imagery, it was super-resolved using ESA SNAP.

Sentinel-2 Super Resolution is a plugin created by Brodu (2017) for the ESA SNAP application that allows all bands within a Sentinel-2 image to be downscaled to 10 m from 20 or 60 m. The super resolution plugin works by using the 10 m bands in the same way a panchromatic band would be used to pan-sharpen an image. The plugin was quite computationally intensive to use (for example, a test was done using an image that covered the whole island – in this situation it took ~1 hour to super resolve just one band of that image) so, in the interest of time, it was only used on a small area of the island – for these images the super resolution took ~20 minutes per band. This plugin was used on the downloaded Sentinel-2 imagery so that the water index equations could be completed. Without downscaling the 20 and 60 m bands the indices would not have worked as all bands involved are required to be of the same resolution. The process of using the plugin was overall very simple – the desired image was selected in the plugin window and the size of the subset was entered using cell values. The resulting super-resolved images were used to complete the water index calculations – this process will be described later in this chapter.

There have been other studies where the 20 and 60 m bands in Sentinel-2 have been downscaled using other methods (e.g. Park et al., 2017), however, the SNAP super resolution was the simplest way to do this for this study as the downscaling process was not the focus. This method, while effective overall, was limiting in that only very small images could be used for the processing to be completed in a reasonable timeframe, meaning a 'pre-selection' of areas of interest had to be made. Larger images were first tested, however the processing time, as mentioned previously, meant it would have taken too long given the number of images that required processing.

After the super-resolution was completed, the water indices were calculated, and the results were mosaicked together using the ENVI 5.5 Seamless Mosaic tool. The mosaicking could not be completed prior to these tasks because the tool was unable to include more than four image bands, but there were more than four that were necessary for some of the water index calculations.

Most of the processing analyses of the Sentinel-2 data were completed without removal or exclusion of any cloud, however it was upon further post-processing analyses that it was necessary for cloud removal to be completed. This cloud-removal process will be discussed later in this section.

The analyses that were completed after the clouds were removed from the images included creating histograms for each individual image. Similarly, to the Planet analysis, an ArcGIS toolbox was created specifically to do this. For Sentinel, however, the toolbox did not automatically extract the clouds from each image as there was no associated file to include as there was with Planet. The ArcGIS toolbox sorted pixels for each individual image into 200 bins between -1 and 1, and these files could then be opened as a .csv file in Excel and be used to create the histograms.

4.2.3 Landsat 8

As the Landsat data had the lowest spatial resolution, it was necessary to downscale it so that it could be at a similar resolution to Sentinel or Planet. To complete this, the data was pan-sharpened In ENVI 5.5. using the NNDiffuse method (Sun et al., 2014). All of the automated sharpening tools available in ENVI were first tested to see which was most effective in providing the clearest resulting image, and it was NNDiffuse which was found to be the simplest (least amount of steps taken to complete), with the clearest image.

Subsets of the Landsat 8 data were created so that each downloaded image surrounded the island and a small amount of water only. The subset was created using a Sentinel-2 subset as a mask so that all images were of the same size. This step was necessary so

that water index calculations were not being completed on pixels that were not part of the area of interest.

Creation of Landsat 8 AWEI histograms

Using the Histogram Data toolbox in ArcGIS Pro, the minimum and maximum values were changed to -50,000 and 50,000 respectively. The reason for this is due to the Landsat 8 reflectance values being much higher than the comparable Sentinel-2. When the reflectance values are entered into the AWEI equations, the result equates to a number in the 10s or sometimes 100s of thousands. Therefore, the regular -1 and +1 minimum/maximum values cannot be used as there are very few or no pixels in the resulting images with these values.

4.3 Water index calculations

Each water index was calculated for the images using Band Math in ENVI 5.5. In this tool, the equation is inputted, and then the required bands are selected from within the image. This allowed for easy adaptation of each equation depending on which bands were required for the different datasets. The water indices used were:

- Normalised Difference Water Index (NDWI)
- Modified Normalised Difference Water Index (MNDWI)
- Automated Water Extraction Index ($AWEI_{nsh}$ and $AWEI_{sh}$)
-

As shown, the equations for each water index (Sections 2.3.1, 2.3.2, & 2.3.3) make use of a number of different bands. For example, the $AWEI_{sh}$ equation required the blue, green, NIR, SWIR1 and SWIR2 bands, which for Sentinel 2 was bands 2, 3, 8, 11 and 12 respectively, but for Landsat 8 was bands 2, 3, 5, 6 and 7 respectively. The use of ENVI's Band Math made it simple to adjust the equations when necessary as the same equation could be used for each dataset even when the required bands were different. The bands are selected directly from the image after the equation is chosen, which meant the equation did not have to be rewritten to account for each new dataset. Because the bands of the Sentinel-2 images had previously been 'Super-resolved,' when they were calculated upon, the individual bands had to be opened as separate images, rather than one image containing all the necessary bands. The resulting water index images were grey scale and contained only one band which was the water index equation.

4.3.1 NDWI

The normalised difference water index (NDWI) is an equation which is calculated on a satellite image to try to delineate open water features of the image (McFeeter's, 1996). It is based on similar ideas as the normalised difference vegetation index (NDVI), which aims to highlight vegetated areas of an image, but by reversing the NDVI equation, open water features can instead be highlighted instead.

The NDWI equation is as follows:

$$NDWI = \frac{(Green - NIR)}{Green + NIR}$$

Band specifications can be viewed in table 4

Platform	*Green band*	*NIR band*
Sentinel-2	3 (541.8 nm - 577.8 nm)	8 (779.8 nm - 885 nm
Planet	2 (515 nm - 595 nm)	4 (740 nm - 900 nm)
Landsat 8	3 (525 nm - 600 nm)	5 (845 nm - 885 nm)

TABLE 5 BAND SPECIFICATIONS FOR EACH SATELLITE PLATFORM WHEN USED WITH THE NDWI WATER INDEX

The near infrared band is used because water strongly absorbs NIR and vegetation strongly reflects NIR. The green band is used because it holds reflected green light, and these green wavelengths are able to maximise the reflectance of water. Overall, the equation should 1) maximise the typical reflectance of water features by using green light wavelengths, 2) minimise the low reflectance of NIR by water features, and 3) take advantage of the high reflectance of NIR by terrestrial vegetation and soil features. Once an image has been processed with the equation, water features will have positive values while soil and terrestrial vegetation features will have zero or negative values.

4.3.2 MNDWI

The modification of normalised difference water index (MNDWI) was created as the NDWI supposedly cannot effectively distinguish between built-up land noise and extracted water features which causes them to become mixed up. This is because the green band and the NIR band have a similar reflectance pattern for built-up land and water, where they both reflect green light more than they reflect infrared light. This results in positive values for both water and built-up land.

The MNDWI equation is as follows:

$$MNDWI = \frac{(Green - MIR)}{(Green + MIR)}$$

Band specifications can be viewed in table 5

Platform	*Green band*	*MIR (SWIR) bands*
Sentinel-2	3 (541.8 nm - 577.8 nm)	11 (1567.5 nm – 1659.2 nm) 12 (2114.9 nm – 2289.9 nm)
Planet (not used for MNDWI)	2 (515 nm - 595 nm)	NA
Landsat 8	3 (525 nm - 600 nm)	6 (1560 nm – 1660 nm) 7 (2100 nm – 2300 nm)

TABLE 6 BAND SPECIFICATIONS FOR EACH SATELLITE PLATFORM WHEN USED WITH THE MNDWI WATER INDEX

4.3.3 AWEI

The Automated Water Extraction Index (AWEI) was created to try and improve the accuracy of surface water mapping by automatically suppressing classification noise from shadow and other non-water dark surfaces, and also to test how effectively this new method would work under different environmental conditions and to compare it against existing methods. When the AWEI was created, the images used were of various water bodies in different areas and conditions from five different countries. It is important that a range of test sites were used as this would ensure that the equation would work with accuracy no matter what the conditions of the image were like. To maximise the separability of water and non-water pixels, band differencing, addition, and the application of different coefficients were used. This has resulted in the creation of two separate equations to ensure maximum effectiveness.

The two AWEI equations are as follows:

$$AWEInsh = 4 \times (\rho green - \rho SWIR1) - (0.25 \times \rho NIR + 2.75 \times \rho SWIR2)$$

$$AWEIsh = \rho blue + 2.5 \times \rho green - 1.5 \times (\rho NIR + \rho SWIR1) - 0.25 \times \rho SWIR2)$$

Band specifications can be viewed in table 6

Platform	*Green band*	*Blue band*	*NIR band*	*SWIR bands*
Sentinel-2	3 (541.8 nm - 577.8 nm)	2 (459.4 nm – 525.4)	8 (779.8 nm - 885 nm	11 (1567.5 nm – 1659.2 nm) 12 (2114.9 nm – 2289.9 nm)
Planet	2 (515 nm - 595 nm)	NA	4 (740 nm - 900 nm)	NA
Landsat 8	3 (525 nm - 600 nm)	2 (450 nm – 515 nm)	5 (845 nm - 885 nm)	6 (1560 nm – 1660 nm) 7 (2100 nm – 2300 nm)

TABLE 7 BAND SPECIFICATIONS FOR EACH SATELLITE PLATFORM WHEN USED WITH THE AWEI WATER INDICES

The coefficients used in the equations and the arithmetic combinations of the bands were chosen based on the reflectance properties of different land cover types. Particular importance was placed on the need to enhance the separability of water and dark surfaces such as shadow and built-up areas as they are often difficult to distinguish as they have similar reflectance patterns. The coefficients were also chosen so that non-water pixels would be forced below zero, and water pixels above zero in order to increase the stability of the equations.

The $AWEI_{nsh}$ equation should effectively eliminate non-water pixels, including dark built surfaces in areas with urban background and is best used for areas without shadow. The $AWEI_{sh}$ helps to improve accuracy by removing shadow pixels that $AWEI_{nsh}$ may not be able to, so is best used for areas with shadow and/or other dark surfaces as it could misclassify water surfaces where there are other highly reflective surfaces such as snow, ice, and reflective roof tops in urban areas. In terms of coastline change measurement, both of these indices could be useful; the $AWEI_{nsh}$ where the surrounding environment is open or there are buildings around which are highly reflective. The $AWEI_{sh}$ would be

useful in coastal environments where the surrounding environment is dark with a lot of shadows, such as forested areas.

4.4 Cloud removal

The cloud removal process for the Landsat 8 and Sentinel-2 imagery was the same. Firstly, a cloud mask was created in ENVI using the 'Create Cloud Mask Using Fmask' tool. The tool uses the thermal and cirrus bands within the multispectral imagery to create the cloud mask. The resulting mask is a raster image where non-cloud pixels have a value of 1, and cloud pixels have a value of 0. As the cloud masking tool needed to be completed using the original downloaded multispectral image, once completed, they were saved as a smaller image to match the size of the water index images.

The next step was to use the cloud mask images to remove cloud pixels from the water index images in ArcGIS Pro. This was completed by converting the raster images to a polygon so that the cloud pixels could be deleted. However, for some of the cloud mask images, the areas of cloud/non-cloud had to be edited as the cloud mask did not correctly show the true areas of cloud/non-cloud. The editing was completed in ArcGIS Pro by simply moving and/or deleting the vertices of the polygons. Once the cloud/non-cloud areas appeared to be correct (where the entire cloud polygon was outlined rather than just a portion), and the cloud pixels deleted, the mask could then be used to removethe clouds from the water index images. This was completed using the 'Extract by Mask'tool in ArcGIS Pro.

The removal of cloud for the Planet imagery was more complicated than for Landsat 8 and Sentinel-2. Although the Planet imagery contained a UDM file for each image, it was difficult to use this for the removal of the clouds. Unlike with Landsat 8 and Sentinel-2, where the cloud pixels could be removed while keeping the non-cloud pixels, the Planet imagery could not be treated in the same. Therefore, viewable images with the clouds removed were not created for the Planet imagery. Instead, the cloud removal process was completed during the creation of the histograms as previously discussed in 4.2.1.

4.5 Displaying the imagery

After completing the water index calculations on each dataset, the image colours were edited to better represent the data. In ArcGIS Pro, the symbology for each individual water index image was changed, which included a new colour scheme and adjustment of the minimum and maximum values. These values were adjusted to display the colours in the correct range for the water indices (-1 to 1) rather than from the true minimum and maximum value that was given after the indices were calculated. The reason for this was so all the image results were the same for a more accurate analysis.

In the literature for each of the water indices the equations give a range of pixel values across the image from -1 to 1. For this study to have the same accuracy as the literature, the values being displayed on the resulting index images must also be from -1 to +1. This does not mean that the results *were* ranging from -1 to +1, however.

4.6 Land/water thresholds

After completing the water index analysis for the images, it was necessary to find out what values within the respective water indices could be considered as 'definitely water' or 'definitely land.' To do this, the same calculations that were used by Cooley (2017) were used. The calculations are as follows:

$$LL = heightlp - 0.9 \times promlp$$

$$WL = heightwp - 0.9 \times promwp$$

Where $height_{lp}$ and $height_{wp}$ are the heights of the peaks of the Excel graphs for land/water respectively, and $prom_{lp}$ and $prom_{wp}$ are the prominences of those peaks. The height of the peak is a measurement from the lowest point of the peak (e.g. the x-axis) to the maximum point of that peak, and the prominence of the peak is the minimum required value from the top of the peak to the trough, at a point where the next peak can begin to be climbed.

The histograms that were created for the NDWI images of all three satellite platforms resulted in a line for each image date on one graph, but this was not suitable for use with the threshold equations. Instead, as done in the Cooley et al. (2017) study, an "average graph" was created, by finding the average of each NDWI value across all the image dates and plotting these to create a new histogram. Because the new histogram was representative of all the NDWI data, it could be used to define the water and land thresholds for the individual dates.

4.7 Image classification

After calculating the land/water thresholds for each of the images, these thresholds were used to 'classify' the images. It was not necessary to complete any supervised or unsupervised classification processes for the images, as the information needed to group the pixels into different landcover types had already been attained. The threshold values were used to display the NDWI images showing three clear pixel types: land, water, and mixed pixels. This was completed in ArcGIS Pro by editing the symbology for each image so that the 'Classify' symbology type was selected, showing three groups, with each group displaying a different pixel type. For example, pixels with values between 0 and -0.23 displayed as green for vegetation, pixels with values between 0.23 and 0.46 displayed as grey for mixed pixels, and pixels between 0.46 and 1 displayed as blue for water pixels.

5 IDENTIFYING AND COMPARING LANDSCAPE CHANGE

5.1 Visual comparison of water indices

The grid in figure 6 provides a comparison of all water indices across all satellite platforms, where the spatial resolution of Sentinel-2 is 10 m, of Planet is 3 m, and of Landsat 8 is 15 m. To allow for the most accurate comparison, all images used were either from the same date (05/12/2018) or the closest available date to it. This date was chosen as it was during a time when there was minimal cloud-cover in the images across all platforms. The blank spaces in the Planet column show water indices that could not be calculated as the required image bands were not available with the Planet data. Colour contrast differs across each platform and between indices, where some images have more vibrant colours, and others have more dull colours. This is due to the different spectral responses and bandwidths for each satellite platform but could also be affected by atmospheric interference at the time of capture.

The RGB images show an area of coastal aggradation (A, B, C in Figure 6, ~8 km x ~5 km) that is identifiable for each platform. The ability to identify this region will be used to compare the indices and platforms and will help to determine which is the most effective when measuring coastal change. The colouring of the images will help to determine this, as colouring on all index images is scaled to identify water, land, and areas of sedimentation (mixed pixels). Blues denote water, green land/vegetation, and white pixels indicate mixed areas (land/water) on the coastal interface, or clouds. A cloud-covered region is also visible in the South-East of the Landsat and Planet images, which can be used to evaluate the effectiveness of the indices underpartial cloud cover.

NDWI

Figure 6 displays an example of the NDWI image results across the three satellite platforms taken from a similar date. The Sentinel-2 NDWI result provides an image in which the area of aggradation is visually well-defined. In the Sentinel-2 image, there are three distinct colour profiles and the image has the greatest contrast between the three colours. The area of aggradation is defined by the white colour and due to the high

contrast of the blue and green colouring, this area stands out well, which makes it easy to distinguish where the coastal sedimentation has occurred. For this reason, it is the Sentinel-2 that has provided the best NDWI image results.

The Planet NDWI image is also made up of the same three colour profiles as the Sentinel-2 image, however the colours are not as distinct or as contrasted. Unlike the Sentinel-2 image, the area of coastal sedimentation cannot be easily identified so it is difficult to interpret what the image is displaying. The image is lacking contrast between the blue and green colours, and overall, the colour of the vegetation is more white than green, creating further confusion. The area of aggradation is mostly displayed as blue, which does visually stand out from the vegetation, however, this would also suggest that the aggradation is an area of water which is incorrect.

The Landsat-8 NDWI image also displays three clearly separate colour profiles, with relatively good contrast between the colours, but less than that of the Sentinel-2 image. This could be due to atmospheric interference or the spectral response of the satellite sensor on the different types of land cover. The area of coastal sedimentation can be identified visually but is more difficult to see than in the Sentinel-2 image due to the overall clarity of the image. If the spatial resolution of the satellite was at the same level as Sentinel-2, these two images may have been more equal in their ability to offer an image where the area of coastal aggradation is clear and well-defined.

MNDWI

The Sentinel-2 MNDWI image has three distinct colour profiles with high contrast between them. In the image, the area of coastal sedimentation can be easily identified as it is represented by the white colour in the image. Compared to the Sentinel-2 NDWI image, the water pixels in the MNDWI image have less contrast, which makes the sedimentation pixels along the coastline a little more difficult to distinguish than in the NDWI image. For this reason, the NDWI index is visually better than the MNDWI index.

The Landsat-8 MNDWI image is made up of three colours, however the contrast between the blue and green colours is the lowest out of any of the images across all platforms and

indices. The reason for this could be due to the low spatial resolution of the satellite combined with the bands that were required for this equation, which are the Middle Infrared and Green bands. As well as this, the bandwidth of the Landsat MIR band is much wider than that of the Landsat NIR band. The use of the MIR band is usually used to help better distinguish built-up land areas from vegetation, but as there is no areas of built-up land in any of the images, the resulting image did not display an accurate pixel distribution.

$AWEI_{sh}$

The Landsat 8 image for this index has the highest contrast between the blue and green colours out of all the indices for this platform. However, the clouds for this date did affect the resulting image somewhat, as sections of the cloud cover have been confused for water pixels. In the Sentinel-2 image, the contrast between the blue and green colours is less than that of the NDWI and MNDWI, but there appears to be greater differentiation within the vegetation area specifically, as there are areas of darker greens and lighter greens. The likely reason for this is that the $AWEI_{sh}$ index is designed for use where there is a lot of shadow or dark features, which would be the case for these images due to the extensive vegetation. The reason this index is designed for shadowy areas is due to the bands and coefficients used in the equation. The bands used include blue, green, SWIR1 and SWIR2. The coefficients within the equation are the numbers 2.5, -1.5, and 0.25. The purpose of the inclusion of the coefficients is to increase the separability of the water and non-water pixels, which should therefore produce more negative or more positive values respectively.

$AWEI_{nsh}$

The two images in figure 6 displaying the $AWEI_{nsh}$ index show how this index has much different appearance for their respective platform compared with the other indices of that platform. For Sentinel-2, there is less contrast between the blue and green colours compared with the other indices, and for Landsat-8, it is the differentiation of the colours that has been affected. The likely reason this has occurred is because the $AWEI_{nsh}$ platform was designed for use in areas with a significant amount of built-up or urban areas. There is very little or no built-up or urban areas in the area displayed in the images,

so the index has less applicability. It was still chosen for use in this situation so that there was a full comparison of available water indices. It is interesting to note that in the Landsat-8 $AWEI_{nsh}$ image, the clouds have somewhat disappeared. This could be because the clouds would have had a similar reflectance as urban areas, creating confusion when the index was calculated. As with the AWEIsh equation, there are coefficients involved with AWEInsh which are combined with the bands used to create more negative and more positive values for certain pixels. The bands used in this equation are green, NIR, SWIR1 and SWIR2, with coefficients 4, 0.25, and 2.75.

Summary

The MNDWI and AWEI indices were formulated for areas where built-up land negatively affected results of the NDWI. Their ability to lessen the impact of built-up land is due to the reflectance pattern of this type of landscape. Both water and built-up land reflect light more than they reflect NIR light, which is why in the MNDWI and AWEI indices these two land types would have positive values. This would result in an image which would appear to have a greater presence of water, but it could actually just be a mix of those pixels. However, as there were no areas of built-up land in the images used, this was not an issue of concern.

The NDWI is the only index selected for further evaluation and analysis in this section, as it is overall the most appropriate index for the environment. The NDWI images were chosen because this index is highly visually contrasted which has provided measurable results out of all water indices, and it is the only index which could be used across all three platforms. Overall, the NDWI images provide the greatest contrast between colours – particularly with the Sentinel sourced imagery – as well as providing the best visibility of the sediment development after the eruptive episodes (Figure 7). It is likely that the environment of Ambae, e.g. almost unbroken vegetation, is the reason why NDWI was the most effective index. The use of the NIR band in the index is used to minimise the low reflectance of NIR by water and to maximise the high reflectance of the NIR by vegetation and soil (Xu, 2006).

As well as this, it is selected for its ability to differentiate regions of coastal aggradation,

water and land; availability across all pixels, and ease of calculation that does not require arbitrary coefficients.

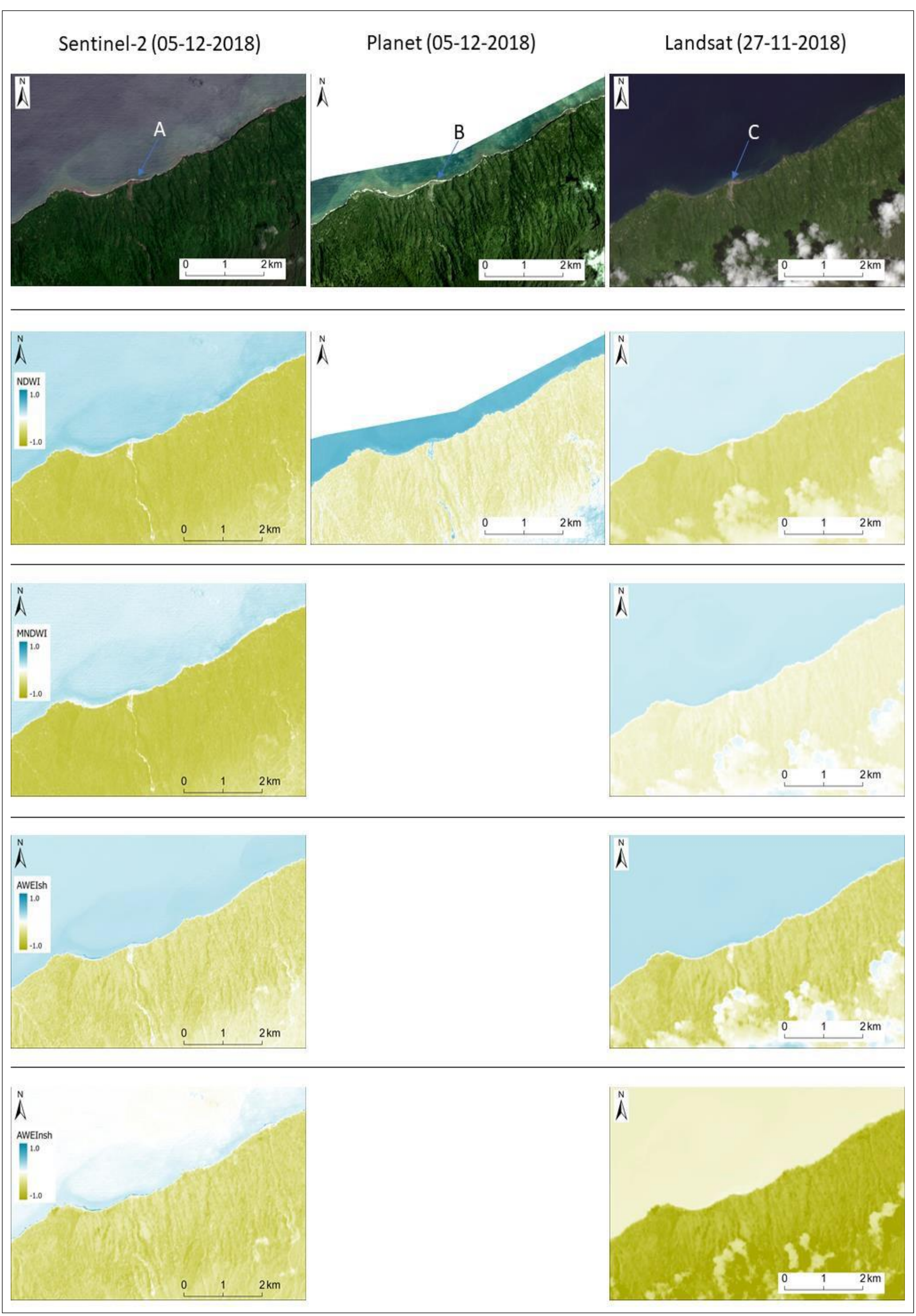

FIGURE 6: THIS TABLE OF FIGURES SHOWS THE RESULTING IMAGERY OF EACH SATELLITE PLATFORM AFTER EACH WATER INDEX WAS CALCULATED. THE IMAGES SHOWN FOR SENTINEL-2 AND PLANET ARE FROM THE SAME DATE, 05/12/2018, AND THE LANDSAT 8 IMAGES ARE FROM 27/11/2018 WHICH WAS THE CLOSEST AVAILABLE DATE TO THE REST. THESE IMAGES WERE CHOSEN AS THEY ARE THE CLEAREST AND LEAST CLOUDY IMAGES FOR EACH RESPECTIVE PLATFORM.

5.2 Timeline of sedimentation

A timeline of NDWI images were created for each of the three satellite platforms. The images used were all those available between the July 2017 and March 2019, covering the pre-eruptive, eruptive, and post eruptive period of activity. The images used were either free from cloud or had the least amount of cloud over the areas of interest. For Planet, the images used were also those which were large enough for display purposes and those which included the areas of interest.

Sentinel Timeline

The images in the Sentinel-2 timeline appear to decrease in contrast between the blue and green colours as time goes on. The one exception to this is the image for 12-08-2018, however this image also has significant cloud cover which is likely to have affected the distribution of pixel values. Another visible change in the images over time is the development of the alluvial fan in about the centre of the images. In the first two images this development is not there, but from the 13-07-2018 image (which was shortly after the most significant eruption episode) onwards it is there. From a visual perspective, the development does appear to increase in size and become smaller again over time, with its visibility much less in the final image dated 24-01-2019, where there is little outward growth from the coastline on this date compared with dates soon after the initial eruption phases.

Planet timeline

The most noticeable aspect of the Planet timeline is the inconsistency in size/location of the images. Planet image footprints are smaller (in area) than Sentinel and Landsat platform footprints, resulting in inconsistencies in image footprint and sizes. The images chosen for the timeline and that were used for the water index calculations were those which best showed the main area of interest (Area A, B, C in figure 6). Overall, the contrast of the Planet timeline is much less than that of the Sentinel timeline. It is also more difficult to see the area of development that is so clearly visible across the Sentinel timeline. Many of the images do have significant cloud cover, however, even in the images with very little cloud cover the development area is more difficult to see.

Landsat Timeline

All images of the Landsat timeline are similar in appearance and are low in contrast, so the colours of the images are pale compared to Sentinel or Planet. The similarity between the images is likely due to the low spatial resolution of Landsat 8 which has made it difficult to identify any distinguishing features in the images. In the images between 03/05/2018 and 27/11/2018 it is possible to see the sedimentation in the main area of interest (Area A, B, C in figure 6), however without knowing where to look, it is not noticeable compared to the Sentinel-2 images. Many of the Landsat 8 images contained a significant amount of cloud cover, which is also a likely reason for the poor quality and low contrast of these images.

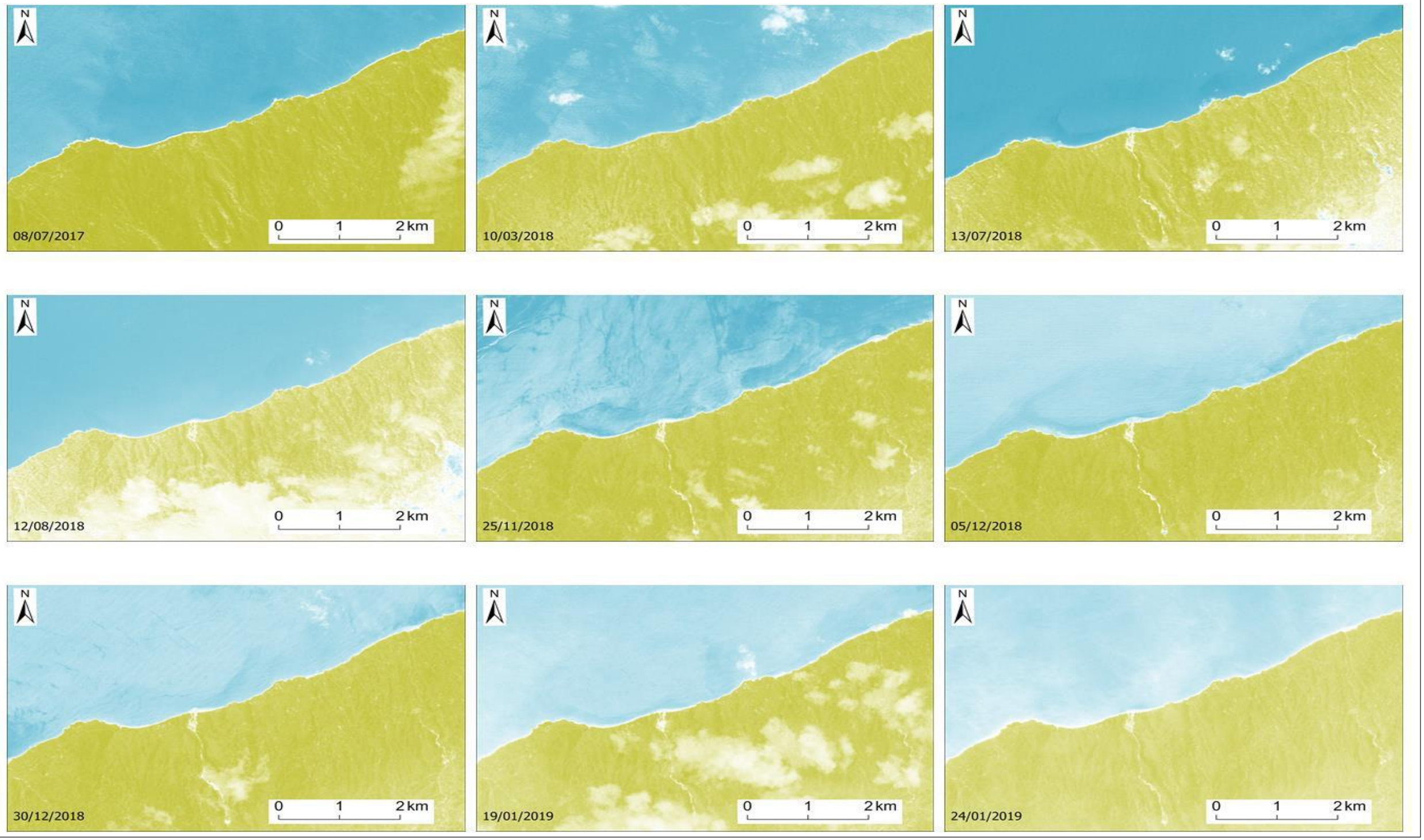

FIGURE 7: THIS SERIES OF IMAGES SHOWS THE CHANGE OVER TIME BETWEEN AUGUST 2017 – MARCH 2019 FOR SENTINEL-2 NDWI IMAGES. THE FIRST IMAGE, DATED 08/07/2017 WAS PRIOR TO THE MOST SIGNIFICANT ERUPTION, AND THE LAST IMAGE, DATED 24/01/2019 IS FROM AFTER THE ERUPTION PHASES HAD ENDED.

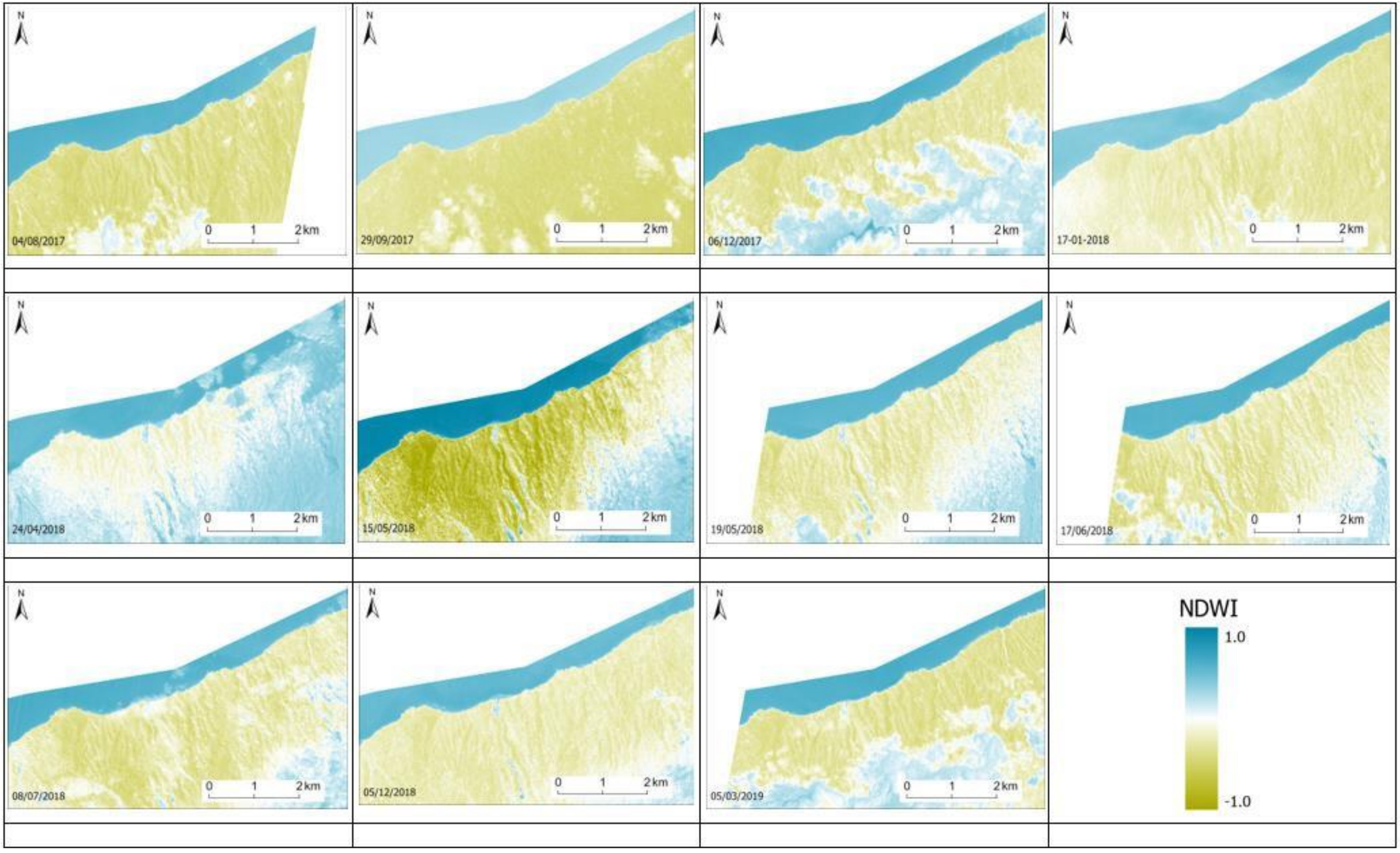

FIGURE 8: THIS SERIES OF IMAGES SHOWS THE CHANGE OVER TIME BETWEEN AUGUST 2017 – MARCH 2019 FOR PLANET NDWI IMAGES. THE FIRST IMAGE, DATED 04/08/2017 WAS PRIOR TO THE MOST SIGNIFICANT ERUPTION, AND THE LAST IMAGE, DATED 05/03/2019 IS FROM AFTER THE ERUPTION PHASES HAD ENDED.

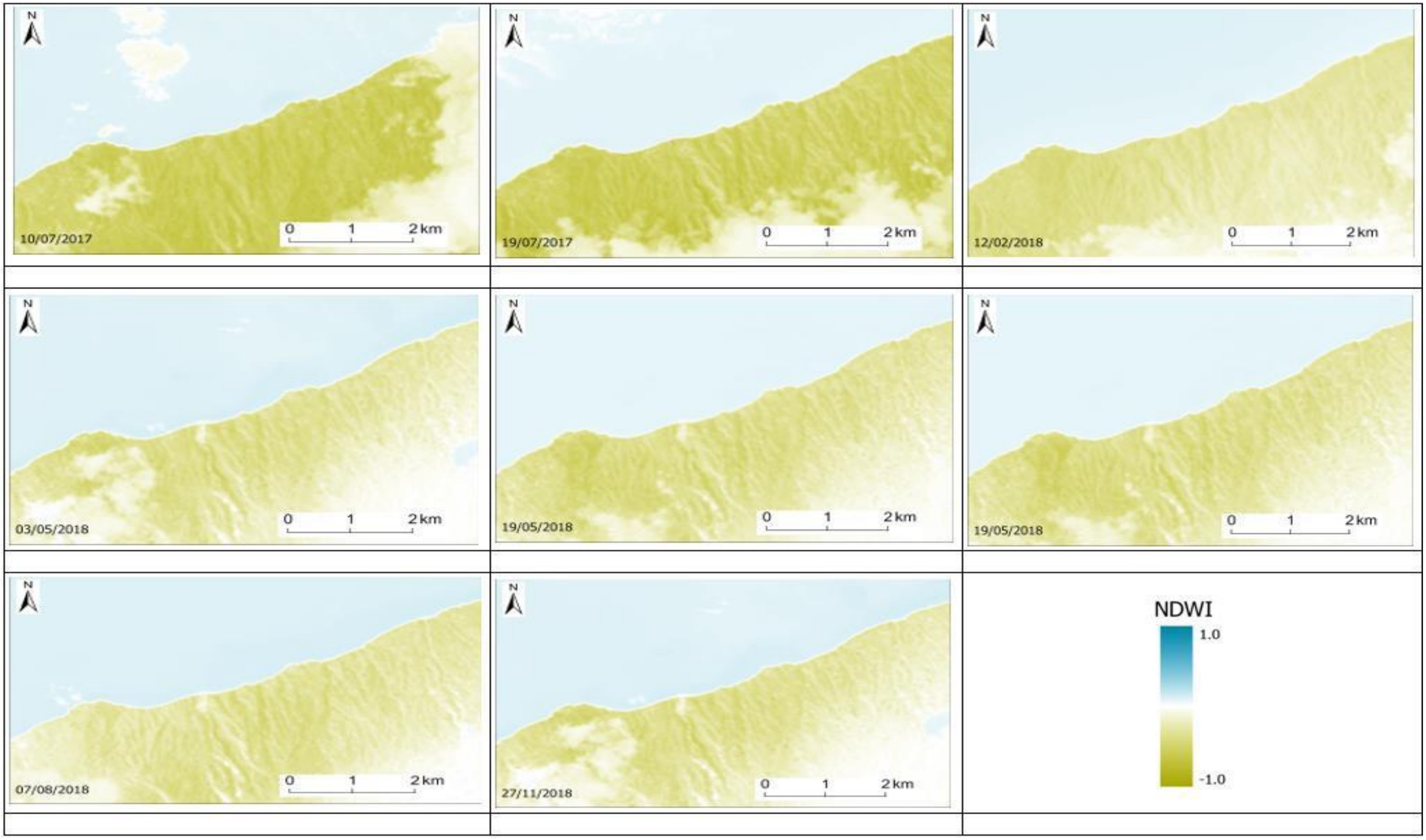

FIGURE 9: THIS SERIES OF IMAGES SHOWS THE CHANGE OVER TIME BETWEEN JULY 2017 – NOVEMBER 2018 FOR LANDSAT 8 NDWI IMAGES. THE FIRST IMAGE, DATED 10/07/2017 WAS PRIOR TO THE MOST SIGNIFICANT ERUPTION, AND THE LAST IMAGE, DATED 27/11/2018 WAS AFTER THE ERUPTION PHASES HAD ENDED.

5.3 Landscape Change Analysis

The NDWI timelines in figures 7-9 provide visual documentation of the growth (aggradation) and dissolution (erosion) of an alluvial fan between July 2017 and March 2019. It was necessary to measure the magnitude of the coastal processes and to determine whether the landscape changes had occurred in response to the volcanic eruption. To do this, the area of 'mixed pixels' were identified, which are those that are not obviously water or vegetation, suggesting that they accumulated due to the aggradation and erosion processes at the coast. To simplify the analysis, the area of interest was restricted to the region surrounding the identified alluvial fan (A, B, C in figure 6).

5.3.1 Thresholds

Cooley (2017) developed a method for NDWI imagery where pixels could be defined as either 100% land, 100% water, or as mixed pixels. The 100% land threshold (LL) and 100% water threshold (WL) was determined as:

$$LL = heightlp - 0.9 \times promlp$$

$$WL = heightwp - 0.9 \times promwp$$

Where $height_{lp}$ and $height_{wp}$ represent the height of each land/water peak, and $prom_{lp}$ and $prom_{wp}$ represent the prominence of each land/water peak.

This method was used to determine the land and water thresholds for the NDWI images of each satellite platform to supplement the visual analysis. An example of the method is shown in Figure 10. In this example from a Sentinel-2 image, land pixels are those with an NDWI value less than ~-0.475 while water pixels are those with an NDWI value greater than ~0.23. The area between these two values cannot be defined clearly as 'definitely water' or 'definitely land.' The purpose of the landscape change analysis is to evaluate the changes (by area) in these mixed pixels. The graphs created to display the land water thresholds for the NDWI data for each satellite

platform are an addition to the visual analysis which provide a quantitative timeline of the sediment processes.

The other graphs below (figures 11 & 13) were created to show the NDWI images of a specific area before and after the eruptive episodes, which is why only three images were used (one line = one image). Each of the graphs are used to display the NDWI pixel distribution across the satellite image they are related to, whether this is Sentinel-2, Planet, or Landsat 8. The NDWI pixel distribution is plotted against the area of each image, which was calculated by taking the number of pixels (from the histogram data extracted from each image) and multiplying this by the pixel size, e.g. 10x10 for Sentinel-2 (as each image is 10m spatial resolution). The graphs were created using a very small subset of the images, so that they would only display information for the most significant area of interest. Creating this subset also meant that there was almost no cloud cover in any of the images, so there was no need to perform cloud masking. Although the clouds were previously removed from the images, creating graphs using the information in those images meant that the area of each image was different, and this did not translate effectively into a graph. By using the very small subset, it ensured that all images used in the graphs were exactly the same size and the area could then be calculated for them and used to compare across satellite platforms.

The first graph displayed in this series (figure 11) shows all the NDWI pixels (on each line) for three Sentinel-2 images used, where the lightest coloured line is from an earlier date pre-eruption and the darker coloured lines are from later dates post-eruption. The images used in this graph were from a clear day, and the dates were selected to clearly compare the changes in the pixel distribution from before the eruption to after the eruption. The graph is effective at displaying what can be seen in the images. The peak in the line is a direct representation of the sedimentation growth along the coastline. The distribution of pixels appears to be quite evenly spread for the Sentinel-2 graph, although the peaks of the land pixels are slightly higher than the peaks of the water pixels. Furthermore, the trough of the graphs, between the two peaks, is the most centralised out of all three graphs, sitting just

below zero. This is perhaps suggesting that the data provided by the Sentinel-2 images is the most “normal” in terms of pixel distribution.

The graphs for the Planet images are similar to the Sentinel-2 graph, with Figure 13 having a select number of dates displayed on the graph. As well as this, the area on the graph where the line directly represents the area of sedimentation has been highlighted. The distribution of pixels is not as evenly spread as the Sentinel-2 graphs – the negative water pixels have lower peaks and a wider range of pixel values, whereas the land pixels have a much higher peak and a smaller range of pixel values. The middle section of the graph between the two peaks is also not very centralised. Where the Sentinel-2 graph trough sits at about zero, the Planet graph’s middle trough sits at about 0.2, so overall, the Planet data has provided a higher range of NDWI pixel values compared with Sentinel-2.

The Landsat 8 graph (Figures 14) were less helpful in representing the images than the Sentinel- 2 or Planet graphs were. Due to the lesser contrast of the Landsat images, the information translated differently into the graph, so they appeared to have a much different pixel distribution than Sentinel-2 or Planet. For example, the portion of thegraph for the land pixels (negative values) are highly peaked and less spread out compared to Sentinel-2 or Planet which is due to the land pixels in the images being more concentrated within a smaller range of values. The Landsat graphs are ineffective at displaying the data in a way that directly represents the sedimentationgrowth. Because the land pixel peaks are so tall, it creates a deficit in the rest of the graph, so the values are not easily visible, especially in the section of the graph between the two peaks. Although the information provided by this graph is difficult to interpret and perhaps not very valuable, the trough does sit at a similar position to that of Sentinel-2, at just below zero.

The graphs show that the range of “mixed pixels” for Planet and Sentinel-2 are very similar, with Landsat having a much smaller range. Sentinel-2 has the largest land

threshold, as calculated using the Cooley (2017) method, at around -0.5, whereas Planet and Landsat have a much smaller land threshold at around -0.2. Conversely, Planet has the largest water threshold at almost 0.6, and Sentinel-2 and Landsat-8 have smaller water thresholds at just over 0.2 and ~0.1 respectively.

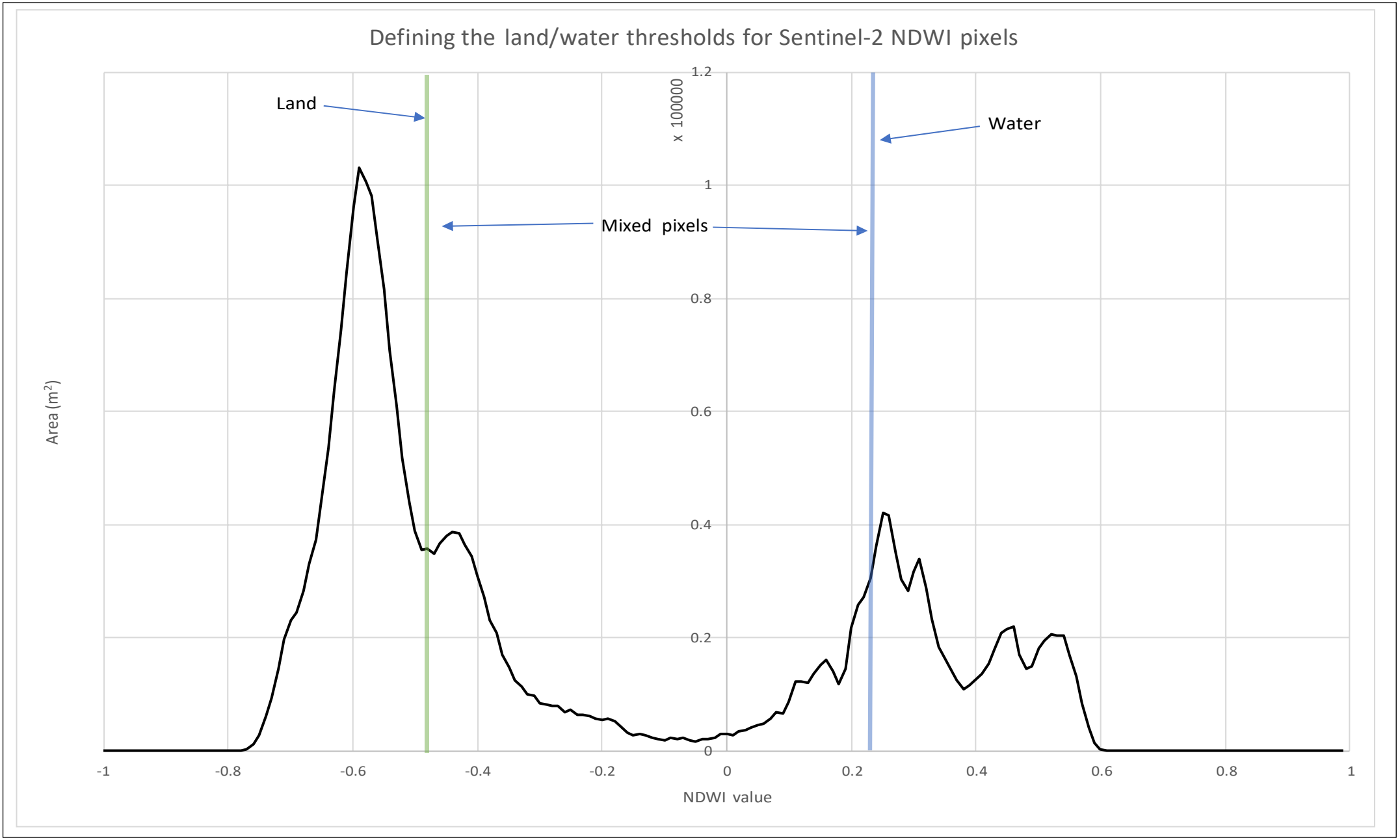

FIGURE 10: THIS GRAPH SHOWS THE LAND/WATER THRESHOLDS FOR SENTINEL-2. THE MIDDLE SECTION OF MIXED PIXELS CANNOT BE DEFINED AS WATER OR LAND. AT THE GREEN LINE AND ALL VALUES BELOW, THE PIXELS CAN BE CONSIDERED AFIGURE 12: THIS GRAPH SHOWS THE LAND/WATER THRESHOLDS FOR PLANET. THE MIDDLE SECTION OF MIXED PIXELS CANNOT BE DEFINED AS WATER OR LAND. AT THE GREEN LINE AND ALL VALUES BELOW, THE PIXELS CAN BE CONSIDERED AS 'DEFINITELY VEGETATION' AND AT THE BLUE LINE AND ALL VALUES ABOVE, THE PIXELS CAN BE DEFINED AS 'DEFINITELY WATER.' THIS GRAPH, HOWEVER, IS MADE UP OF THE AVERAGE VALUES FOR ALL NDWI VALUES COMBINED, AND TO COMPLETE FURTHER ANALYSIS, THE THRESHOLD VALUES FOR EACH INDIVIDUAL NDWI DATE HAD TO BE CALCULATED.

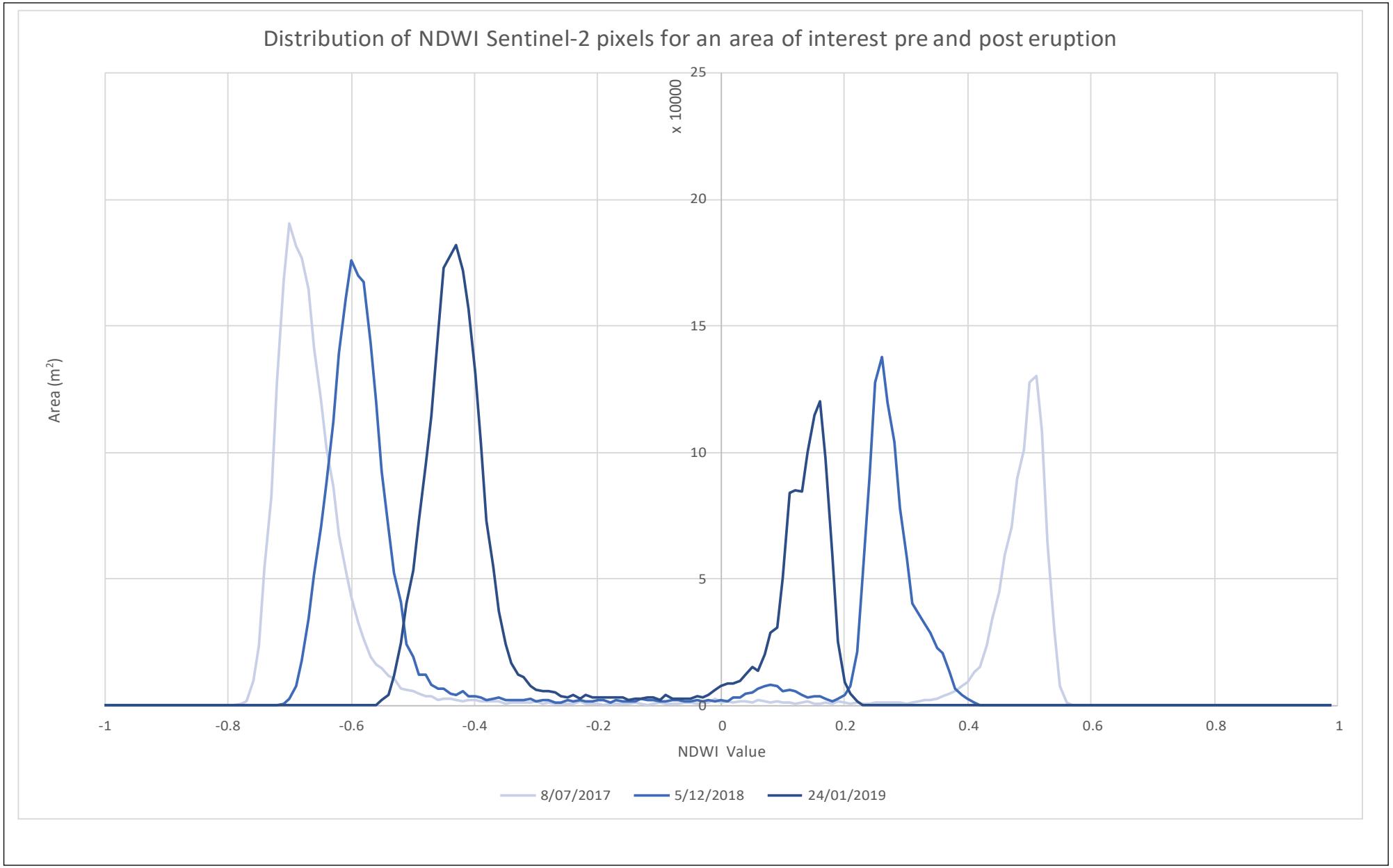

FIGURE 11: THIS GRAPH SHOWS THE DISTRIBUTION OF NDWI PIXELS FOR THREE DATES DURING THE CHOSEN TIMEFRAME: BEFORE THE ERUPTION, JUST AFTER THE ERUPTION, AND SOME TIME AFTER THE ERUPTION PHASES HAD ENDED. THIS GRAPH IS HERE TO SHOW HOW THE DISTRIBUTION OF THE PIXELS HAS CHANGED ACROSS THE TIMEFRAME DUE TO THE DIFFERENT STAGES OF THE ERUPTIONS.

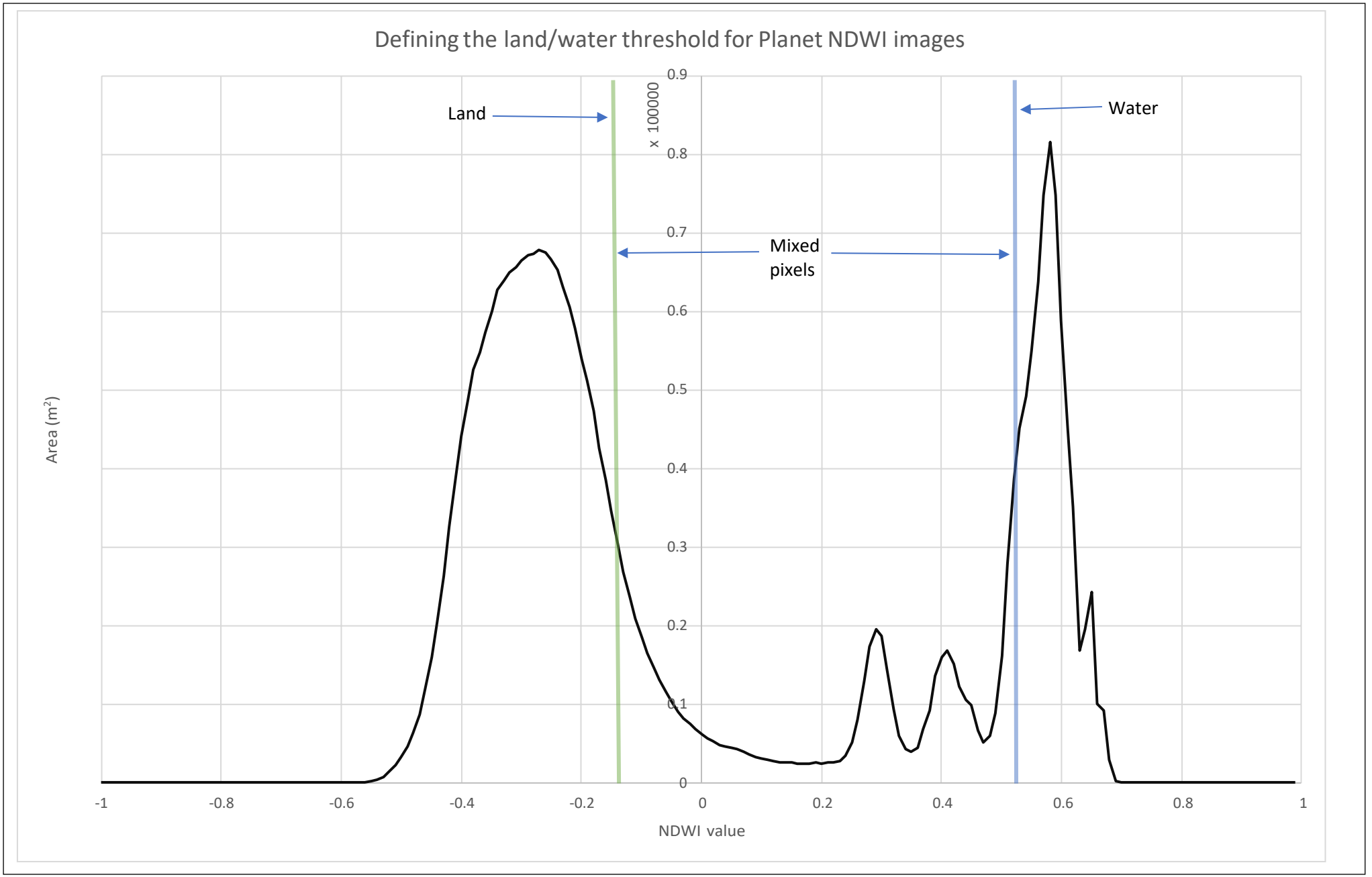

FIGURE 12: THIS GRAPH SHOWS THE LAND/WATER THRESHOLDS FOR PLANET. THE MIDDLE SECTION OF MIXED PIXELS CANNOT BE DEFINED AS WATER OR LAND. AT THE GREEN LINE AND ALL VALUES BELOW, THE PIXELS CAN BE CONSIDERED AS 'DEFINITELY VEGETATION' AND AT THE BLUE LINE AND ALL VALUES ABOVE, THE PIXELS CAN BE DEFINED AS 'DEFINITELY WATER.' THIS GRAPH, HOWEVER, IS MADE UP OF THE AVERAGE VALUES FOR ALL NDWI VALUES COMBINED, AND TO COMPLETE FURTHER ANALYSIS THE THRESHOLD VALUES FOR EACH INDIVIDUAL NDWI DATE HAD TO BE CALCULATED.

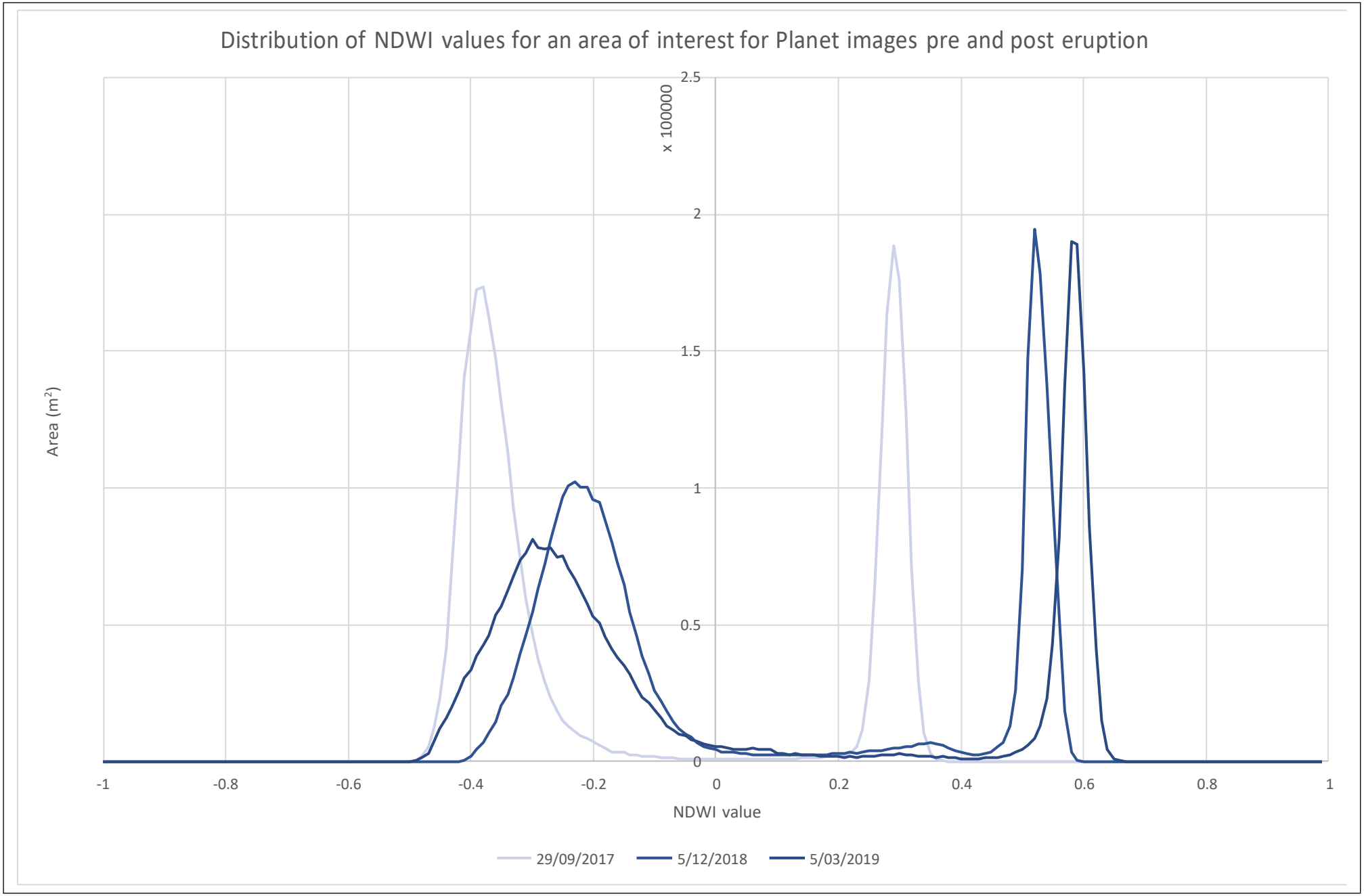

FIGURE 13: THIS GRAPH SHOWS THE DISTRIBUTION OF NDWI PIXELS FOR THE THREE DATES DURING THE CHOSEN TIMEFRAME: BEFORE THE ERUPTION, SHORTLY AFTER THE MAJOR ERUPTION, AND SOME TIME AFTER THE ERUPTION PHASES ENDED. THIS GRAPH IS HERE TO SHOW HOW THE DISTRIBUTION OF THE PIXELS HAS CHANGED ACROSS THE TIMEFRAME DUE TO THE DIFFERENT STAGES OF THE ERUPTIONS.

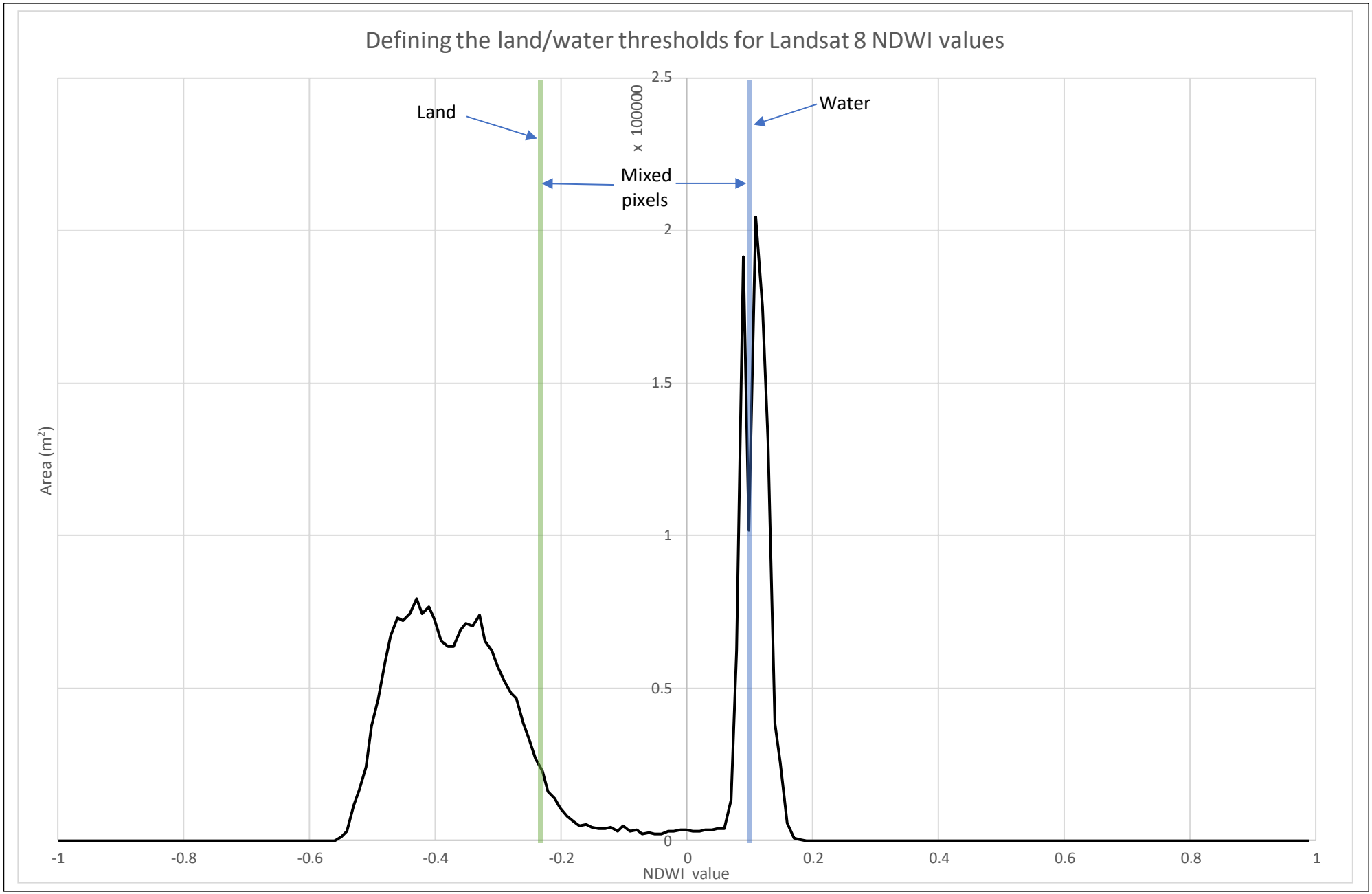

FIGURE 14: THIS GRAPH SHOWS THE LAND/WATER THRESHOLDS FOR LANDSAT 8. THE MIDDLE SECTION OF MIXED PIXELS CANNOT BE DEFINED AS WATER OR LAND. AT THE GREEN LINE AND FOR ALL VALUES BELOW, THE PIXELS CAN BE CONSIDERED AS 'DEFINITELY VEGETATION' AND AT THE BLUE LINE AND FOR ALL VALUES ABOVE, THE PIXELS CAN BE CONSIDERED AS 'DEFINITELY WATER.' THIS GRAPH, HOWEVER, IS MADE UP OF THE AVERAGE VALUES FOR ALL NDWI VALUES COMBINED, AND TO COMPLETE FURTHER ANALYSIS, THE THRESHOLD VALUES FOR EACH INDIVIDUAL NDWI DATE HAD TO BE CALCULATED.

5.3.2 Measuring Landscape Change

The graph in figure 15 shows how the distribution of the mixed pixels has changed over time for each of the three satellite platforms. The graph was created in Excel by first separating the three pixel types (water, mixed, vegetation) into three groups. These groups were delineated using the previously identified thresholds for land (-0.5 for Sentinel, -0.2 for Landsat/Planet) and water (0.2 for Sentinel, 0.2 for Landsat and 0.6 for Planet). The pixel values used for the graph were displayed in m^2 so that the measurements are the same across the three platforms – if they had been displayed as the 'number of pixels' it would skew the data due to the differing spatial resolution of each platform. For example, Planet would have appeared to have a greater number of pixels due to the higher (3 m x 3 m) spatial resolution, and Landsat would have appeared to have far fewer overall due to its lower spatial resolution (15 m x 15 m).

The graph is representative of the NDWI images that have been collected and displayed, where the area of the mixed pixels is low prior to the eruptive episodes (July 2017), and after the first major eruption occurs in July 2018 the mixed pixel area increases significantly.

Sentinel imagery is used as the basis for comparison due to ease of the threshold identification and number of complete captures of the area of interest. A subset of the Landsat and Planet area of mixed pixels are shown for comparison. Results from every platform show a large increase after the major eruptive episode and is not an artefact of the specific platform chosen.

There were only three dates used for the graph lines of the Landsat 8 and Planet imagery so that the graph would not become too complicated The dates selected for the graph were from, before eruptions, just after eruptions, and a longer time after eruptions so they represent the overall time period. It was not necessary to display all of the dates of these two platforms because it is Sentinel that was deemed to be the best satellite platform to use. The other lines were included on the map as a comparison to Sentinel, and they are helpful in confirming that the number of mixed pixels does dramatically increase after the major eruptive episode across all platforms, and is not an artefact of the specific platform chosen.

Sentinel-2 images were classified as land, water, or mixed according to the calculated thresholds and are shown in Figure 10, for the larger region. It is clear for many of the images that certain pixel groups have been mis-classified, for example, cloud pixels. The reason for this is that the cloud pixels lie within the same values as the mixed pixels group. Therefore, the previous analyses for the NDWI distribution graphs and the graph in figure 15 below were created only using a small area within the bigger subset, which shown on the graph. If the larger area had been used, the cloud pixels would have distorted the data and led to inaccurate results. In the smaller area that was used, there was no cloud cover in any of the images across the three platforms.

FIGURE 15: THIS GRAPH SHOWS THE CHANGE IN THE AREA OF MIXED PIXELS FOR THE NDWI IMAGES BETWEEN THE STATED TIME PERIOD. THE VALUES HAVE BEEN CALCULATED FROM THE SMALL AREA AS DEFINED BY THE BOX UPON THE MAP IN THE TOP RIGHTHAND CORNER. THIS SMALL AREA CONTAINED AN AREA OF HIGH SEDIMENTATION BUILD-UP COMPARED WITH OTHER AREAS, AND ALSO MEANT THAT ALL IMAGES USED IN THE CALCULATIONS WERE ENTIRELY FREE FROM CLOUD COVER.

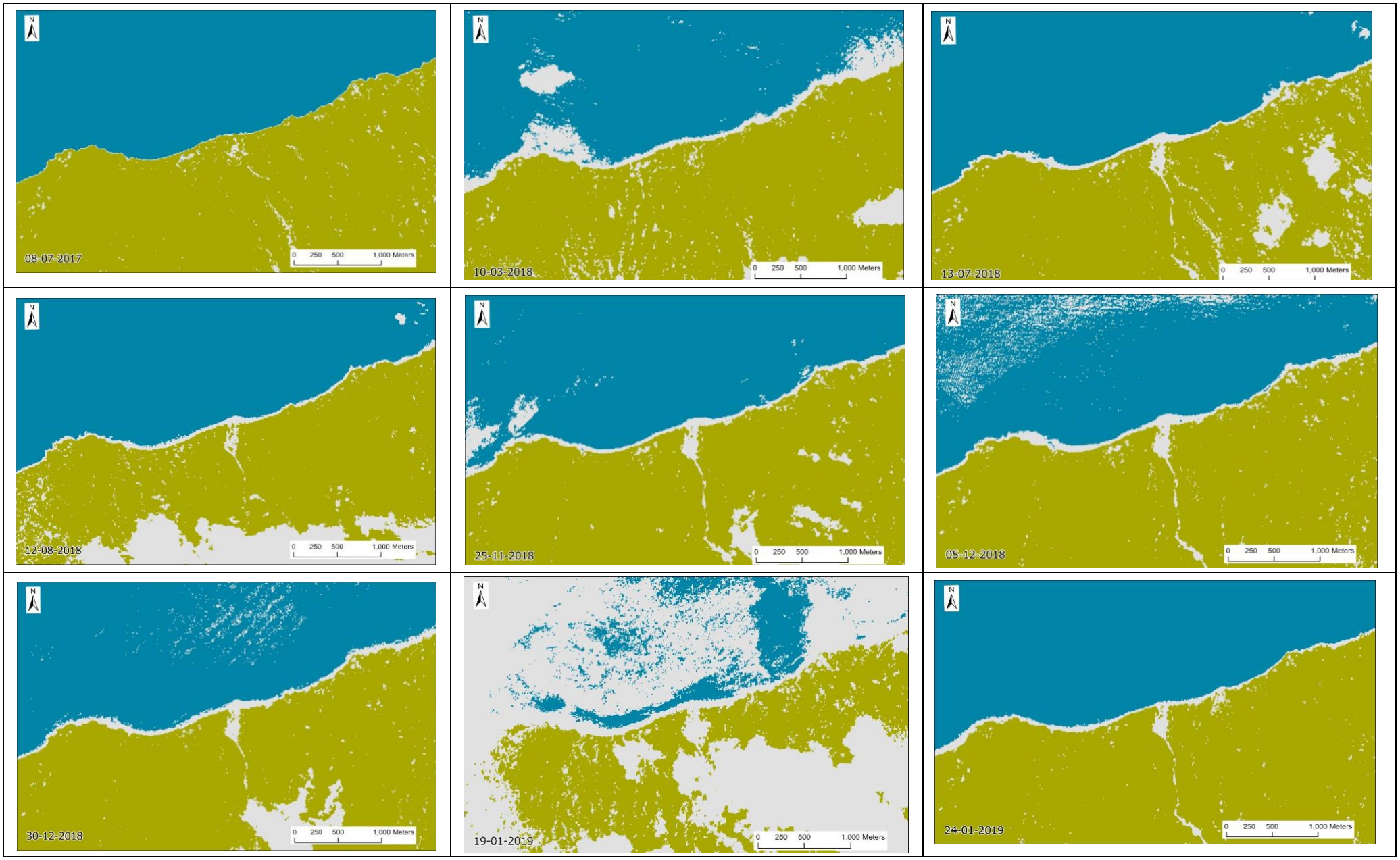

FIGURE 16: THIS SERIES OF IMAGES IS A SIMPLE CLASSIFICATION OF EACH OF THE SENTINEL-2 NDWI IMAGES. THE THREE CLASSIFICATION GROUPS ARE WATER (BLUE), VEGETATION (GREEN), AND MIXED PIXELS (GREY) AND THEY WERE CLASSIFIED USING THE THRESHOLD VALUES FOR EACH OF THE DATES.

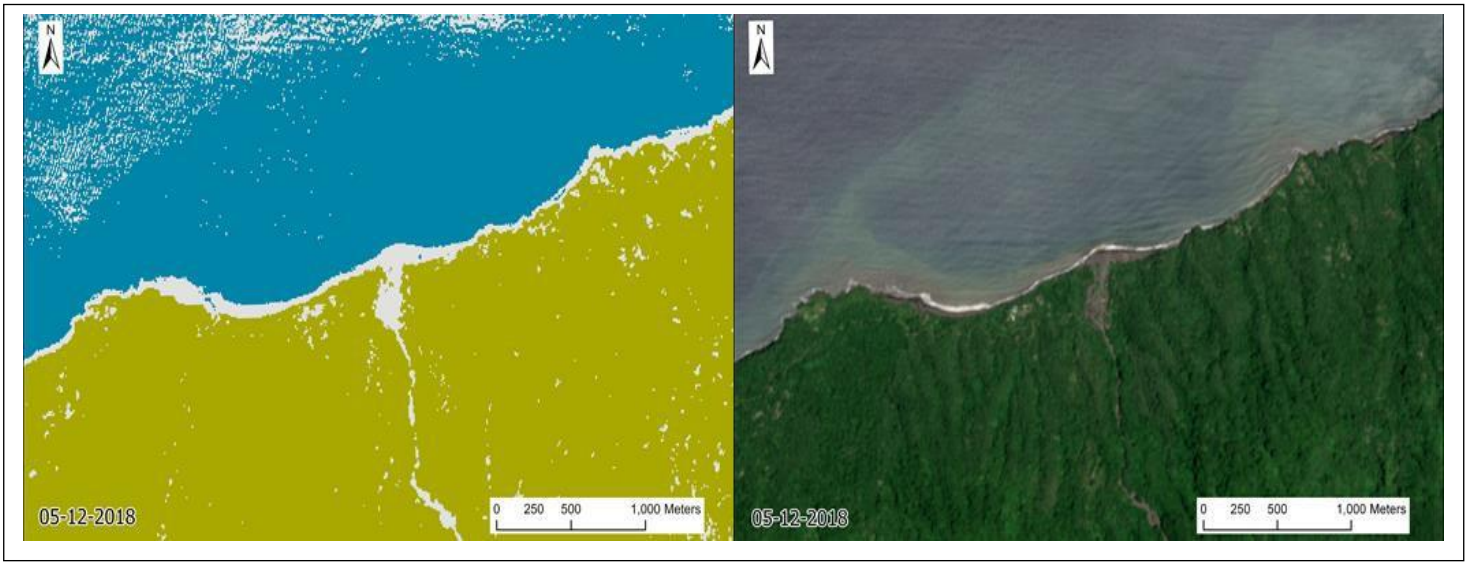

FIGURE 17 A COMPARISON OF THE SENTINEL-2 NDWI IMAGE AND ITS RGB IMAGE FOR 05-12-2018

6 DISCUSSION

6.1 Comparison of image platforms

Sentinel-2 imagery was chosen for use because it had been used previously for similar water index calculation projects, and because it is easy to access while having good specifications. The large number of bands available with Sentinel, and the relatively high 10 m resolution of the imagery made it a good candidate for the completion on the water index analyses. Although not all the required bands were at the 10 m resolution, those that were lower could be "super-resolved" to match the 10 m.

Planet, as opposed to Sentinel-2 and Landsat 8, only has four bands. This was a hinderance to the analyses as it meant only NDWI could be completed with the Planet imagery. As well as this, Planet's high resolution and daily revisit time did not actually contribute any positive significance to the analyses. Figure 5 showed that the clarity across all the images was similar, even though Planet's 3 m resolution would normally provide a much clearer image than Landsat 8's 30 m resolution, which could be explained by the large bandwidths of the Planet imagery. Furthermore, the daily revisit time of Planet did not result in a greater number of high quality, useable images as expected. In the end, there were a similar number of useable images for each platform, which can be seen in the figures that have been provided thus far.

Much of the literature which had completed similar water index analysis methods had used Landsat imagery to do so. In fact, the four water indices, NDWI, MNDWI, $AWEI_{sh}$ and $AWEI_{nsh}$ were first formulated using Landsat imagery (McFeeters, 1996), (Xu, 2006), (Feyisa et al., 2014). This was the main reason why Landsat 8 was chosen alongside Planet and Sentinel-2 for the analyses. However, the results from the Landsat imagery, in comparison to Planet and Sentinel-2, were much poorer. Landsat's low-resolution imagery, even after being pan-sharpened to 15 m, was simply not as effective as Planet or Sentinel-2 at highlighting the areas of interest. The water index images for Landsat 8 all had quite differing contrast than the Sentinel images and the singular Planet image, where, for NDWI and MNDWI, Landsat had less contrast, but for $AWEI_{sh}$, Landsat 8 had greater contrast than Sentinel-2, and for

$AWEI_{nsh}$ the colours of Landsat were different entirely compared with Sentinel-2. It is also unfortunate that most of the Landsat-8 imagery that was downloaded had cloudy areas over the land, which is likely a contributing factor to the contrast issues. However, the cloudy images could not be avoided as they were the best and most appropriate images that were available for download at the time.

6.2 Water indices

The NDWI water index was the most successful of the four that were used as it provided the clearest visible differentiation of the water, vegetation, and mixed pixels. The reason it was the most successful is because the landscape of Ambae, that is, almost entirely unbroken vegetation, is the type of environment the NDWI was formulated for. The other indices used were formulated to be more effective where other landscapes were also involved, such as urban areas, which is why there were a number of different bands used in the equations. The NDWI was also successful as it allowed for a definitive evaluation of how the sedimentation (mixed pixels) changed over the chosen time period by using the information extracted from the images. This success was significant because measuring the change in sedimentation over time was the original aim.

The NDWI was also the most user-friendly water index, equal with MNDWI. The formulae for these two indices were the simplest to input and understand, and the least complicated having only two bands used in each. Both of the AWEI indices required four bands each, as well as multiple coefficients, the value of which are arbitrary. The literature for the AWEI indices did provide an explanation as to why the bands and coefficients were used and what they were supposed to do, but do not appear applicable to this study.

Sentinel-2 was found to be the most useful satellite platform in terms of the imagery it provided. The images were the ‘best quality’ overall when all factors were taken into account, such as the temporal, spectral and spatial resolutions, accessibility of the data, and the area coverage for the images. Sentinel-2 proved that the highest spatial resolution imagery does not necessarily equal the ‘best quality’ imagery. The

likely reason that Sentinel-2 was superior to Planet, for example, is due to the spectral resolution (bandwidth) of the imagery. The bandwidth plays an important role in the appearance of the imagery; for example, Sentinel has a smaller bandwidth for the NIR and green bands, at 106 nm and 26 nm respectively. These are the two bands used in the NDWI equation, and their roles are to minimise the low reflectance of water (using NIR) while maximising the high reflectance of the vegetation (using green) (Xu, 2006). Planet has a bandwidth for 160 nm for the NIR band and 80 nm for the green band, so they are significantly larger than Sentinel's. This is an important factor as it means there is less information provided for the Planet imagery, so it therefore does not look as good. Cao et al. (2018) explains that a broader spectral bandwidth reduces the features of the spectrum, something that has clearly occurred for the Planet imagery, which helps to explain why the contrast between the three pixel-types was lower. It is likely that Landsat 8 would have provided superior results to both Sentinel and Planet, had its spatial resolution been higher, because the bandwidth for its NIR band is only 40 nm, and its green band is only 75 nm.

The Sentinel-2 imagery that was available for download across the desired date range was also, in general, the most evenly spread, and had the least cloud cover over the area of interest. This, however, was more of a factor of luck. For example, the majority of the Landsat 8 imagery available across the timeframe had significant cloud-cover, so it was just bad luck that the days on which the images were captured happened to be cloudy days. The higher number of very cloudy imagery for Landsat 8 meant it was necessary to be more selective with the chosen images; this resulted in less images overall, a smaller time-range of images, and images that were less evenly spread across the whole timeframe.

The spatial and temporal resolutions played an interesting role in the overall data when placed against the spectral resolution and area of coverage for the imagery. It was disappointing that although Planet was expected to provide the best imagery due to its high spatial resolution and almost-daily return time, this was simply not the case. There was somewhat of a 'trade-off' between these factors, where to have a high spatial resolution, other factors were sacrificed that were just as important.

Planet's almost-daily return time should, in theory, have resulted in a greater chance of acquiring cloud-free imagery. This, however, was not the case as both the area coverage of the island and the cloud cover of the images meant this high return time could not be utilised. For much of the imagery, the increase in the number of available images just meant there was an increase in the number of cloudy images, and because the coverage of the images over the island was so inconsistent, many of the images could not even be considered for use. For example, there were a great number of images where only a very small portion of the island had been captured, or in other cases it was half the island, but not the half with the area of interest. It was the inconsistency of this coverage area that meant all the Planet images had to be inspected individually. Contrary to this, Sentinel-2 was highly consistent and the large image footprint meant the same area was always covered and the images were all the same size, and so, although the return time was not as frequent, this was far more beneficial for selecting the imagery and for the project overall.

7 CONCLUSION

The aim of this research was to determine the magnitude of change in sedimentation along the coastline of Amabe, Vanuatu over a ~one-year time period. By completing various analyses using remote sensing imagery, it was determined that there was a significant increase in sediment accumulation that was mostly deposited after the major eruption of Ambae in July, 2018. Sedimentation fluctuated over the months following the eruption, and then receded. The changes in coastal sediment cover over the timeframe allowed for a comparative analysis of satellite platforms (Landsat 8, Sentinel-2, PlanetScope) and water indices (NDWI, MNDWI, AWEI). As well as this, the combination of multiple satellite platforms with water indices allowed for an in-depth comparative analysis of the study area. Completion of the comparative analysis indicated that the Sentinel-2 platform combined with the NDWI index were the most appropriate for this study area. A quantitative measure of land change across the timeframe was enabled by the identification of land and water from the NDWI index. The land/water identification was enabled by the differentiation of individual land and water pixels during the NDWI water index process. Regardless of platform, all results indicated a significant increase in sedimentation following the major eruptive event at Ambae.

The analysis of methods used were helpful in determining the level of change, and they allowed for the development of statistically representative visual aids to complement the images which show the growth of the sediment build-up. The methods used were not specific to the application in which they were used, nor were they specific to usage within volcanic landscapes. For this reason, such methods could be used elsewhere, and applied in other situations where water is involved. If applied to situations within New Zealand, the methods would be just as effective. For example, the NDWI index could be used to find the distribution of water bodies in an area where there is high vegetative cover and where other land cover types are low (the literature suggests that the NDWI may not be as effective where urban areas or

similar are involved). If the environment involves multiple land cover types, then another water index could be used, such as MNDWI or AWEI, as the literature suggests that these are more effective in areas where there is more than just vegetative cover.

REFERENCES

Bani, P., Oppenheimer, C., Varekamp, J. C., Quinou, T., Lardy, M., & Carn, S. (2009). Remarkable geochemical changes and degassing at Voui crater lake, Ambae volcano, Vanuatu. *Journal of Volcanology and Geothermal Research, 188*(4), 347-357. doi:https://doi.org/10.1016/j.jvolgeores.2009.09.018

Brodu, N. (2017). Super-Resolving Multiresolution Images With Band-Independent Geometry of Multispectral Pixels. *IEEE Transactions on Geoscience and Remote Sensing, 55*(8), 4610-4617. doi:10.1109/TGRS.2017.2694881

Bryan, K. R., Kench, P. S., & Hart, D. E. (2008). Multi-decadal coastal change in New Zealand: Evidence, mechanisms and implications. *New Zealand Geographer, 64*(2), 117-128. doi:10.1111/j.1745-7939.2008.00135.x

Cao, W., Twele, A., Plank, S., & Martinis, S. (2018). A three-class change detection methodology for SAR-data based on hypothesis testing and Markov Random field modelling. *International Journal of Remote Sensing, 39*(2), 488-504. doi:10.1080/01431161.2017.1384590

Cao, Z., Ma, R., Duan, H., Xue, K., & Shen, M. (2019). Effect of satellite temporal resolution on long-term suspended particulate matter in inland lakes. *Remote Sensing, 11*(23).

Cooley, S. W., Smith, L. C., Stepan, L., & Mascaro, J. (2017). Tracking dynamic northern surface water changes with high-frequency Planet CubeSat imagery. *Remote Sensing, 9*(12), 21. doi:10.3390/rs9121306

Costa, P. J. M. (2016). Sediment transport. In M. J. Kennish (Ed.), *Encyclopedia of Estuaries* (pp. 562-567). Dordrecht: Springer Netherlands.

Cronin, S., Gaylord, D., Charley, D., Alloway, B., Wallez, S., & W. Esau, J. (2004). Participatory methods of incorporating scientific with traditional knowledge for volcanic hazard management on Ambae Island, Vanuatu. *Bulletin of Volcanology, 66*, 652-668. doi:10.1007/s00445-004-0347-9

Davidson-Arnott, R. (2009). Coastal sediment transport. *Introduction to Coastal Processes and Geomorphology*. Cambridge, Cambridge University Press**:** 139-180.

Dominici, D., Zollini, S., Alicandro, M., Della Torre, F., Buscema, P. M., & Baiocchi, V. (2019). High resolution satellite images for instantaneous shoreline extraction using new enhancement algorithms. *Geosciences, 9*(3). doi:10.3390/geosciences9030123

Du, Y., Zhang, Y. H., Ling, F., Wang, Q. M., Li, W. B., & Li, X. D. (2016). Water Bodies' Mapping from Sentinel-2 Imagery with Modified Normalized Difference Water Index at 10-m Spatial Resolution Produced by Sharpening the SWIR Band*. Remote Sensing, 8*(4), 19. doi:10.3390/rs8040354

Duarte, C. R., de Miranda, F. P., Landau, L., Souto, M. V. S., Sabadia, J. A. B., Neto, C. Â. d. S., Damasceno, A. M. (2018). Short-time analysis of shoreline based on RapidEye satellite images in the terminal area of Pecém Port, Ceará, Brazil. *International Journal of Remote Sensing, 39*(13), 4376-4389. doi:10.1080/01431161.2018.1457229

Feyisa, G. L., Meilby, H., Fensholt, R., & Proud, S. (2014). Automated Water Extraction Index: A new technique for surface water mapping using Landsat imagery (Vol. 140).

Ford, M. (2013). Shoreline changes interpreted from multi-temporal aerial photographs and high resolution satellite images: Wotje Atoll, Marshall Islands. *Remote Sensing of Environment, 135*, 130-140. doi:https://doi.org/10.1016/j.rse.2013.03.027

Gallina, V., Torresan, S., Zabeo, A., Rizzi, J., Carniel, S., Sclavo, M., Pizzol, L., Marcomini, A., & Critto, A. (2019). Assessment of climate change impacts in the North Adriatic Coastal Area. Part II: Consequences for coastal erosion impacts at the regional scale. *Water*, *11*, 1300.

Gens, R. (2010). Remote sensing of coastlines: detection, extraction and monitoring. *International Journal of Remote Sensing, 31*(7), 1819-1836. doi:10.1080/01431160902926673

Global Volcanism Program, 2017. Report on Ambae (Vanuatu). In: Sennert, S K (ed.), Weekly Volcanic Activity Report, 6 September-12 September 2017; 20 September-26 September 2017; 27 September-3 October 2017; 4 October-10 October 2017; 11 October-17 October 2017; 18 October-24 October 2017; 22 November-28 November 2017; 6 December-12 December 2017. Smithsonian Institution and US Geological Survey.

Global Volcanism Program, 2018. Report on Ambae (Vanuatu). In: Sennert, S K (ed.), Weekly Volcanic Activity Report, 14 February-20 February 2018; 14 march-20 march 2018;

18 April-24 April 2018; 23 May-29 May 2018; 4 July-10 July 2018, 25 July-31 July 2018; 29 August-4 September 2018; 19 September-25 September 2018. Smithsonian Institution and US Geological Survey.

Guariglia, A., Buonamassa, A., losurdo, A., Saladino, R., Trivigno, M.L., Zaccagnino, A., & Colangelo., A. (2006). A multisource approach for coastline mapping and identification of shoreline changes. *Annals of geophysics 49*(1).

Hicks, D. M., Shankar, U., McKerchar, A. I., Basher, L., Lynn, I., Page, M., & Jessen, M. (2011). Suspended sediment yields from New Zealand rivers. *Journal of Hydrology (New Zealand), 50*(1), 81-142. Retrieved from http://www.jstor.org/stable/43945015

Horikawa, K. (1981). Coastal sediment processes. *Annual Review of Fluid Mechanics, 13*(1), 9-32. doi:10.1146/annurev.fl.13.010181.000301

Huang, W., DeVries, B., Huang, C., Jones, J., Lang, M., & Creed, I. (2017, 23-28 July 2017). Automated extraction of inland surface water extent from Sentinel-1 data. Paper presented at the 2017 IEEE International Geoscience and Remote Sensing Symposium (IGARSS).

Jawak, S. D., & Luis, A. J. (2015). A rapid extraction of water body features from Antarctic Coastal Oasis using very high-resolution satellite remote sensing data. *Aquatic Procedia, 4*, 125-132. doi:https://doi.org/10.1016/j.aqpro.2015.02.018

Jiang, H., Feng, M., Zhu, Y., Lu, N., Huang, J., & Xiao, T. (2014). An Automated Method for Extracting Rivers and Lakes from Landsat Imagery (Vol. 6).

Jones, H. (2008). Coastal sedimentation: what we know and the information gaps. *Environment Waikato technical report 2008/12*. Environment Waikato Regional Council.

Kaliraj, S., Chandrasekar, N., & Ramachandran, K. K. (2017). Mapping of coastal landforms and volumetric change analysis in the south west coast of Kanyakumari, South India using remote sensing and GIS techniques. *The Egyptian Journal of Remote Sensing and Space Science, 20*(2), 265-282. doi:https://doi.org/10.1016/j.ejrs.2016.12.006

Kourosh Niya, A., Alesheikh, A., Soltanpor, M., & Kheirkhahzarkesh, M. (2013). Shoreline change mapping using remote sensing and GIS case study: Bushehr Province.

Kuenzer, C., & Dech, S. (2013). Theoretical background of thermal infrared remote sensing. In C. Kuenzer & S. Dech (Eds.), *Thermal Infrared Remote Sensing: Sensors, Methods, Applications* (pp. 1-26). Dordrecht: Springer Netherlands.

Lu, D., Mausel, P., Brondízio, E., & Moran, E. (2004). Change detection techniques. *International Journal of Remote Sensing, 25*(12), 2365-2401. doi:10.1080/0143116031000139863

Lyon, J., Yuan, D., Lunetta, R., & Elvidge, C. (1998). A change detection experiment using vegetation indices. *Photogrammetric Engineering and Remote Sensing*, *64*.

Maglione, P., et al. (2014). "Coastline extraction using high resolution WorldView-2 satellite imagery." *European Journal of Remote Sensing 47*, 685-699.

Manolakis, D., Lockwood, R., & Cooley, T. (2016). *Hyperspectral Imaging Remote Sensing*.

Manville, V., et al. (2005). "Fluvial responses to volcanism: resedimentation of the 1800a Taupo ignimbrite eruption in the Rangitaiki River catchment, North Island, New Zealand." *Geomorphology, 65*(1): 49-70.

McFeeters, S. K. (1996). The use of the Normalized Difference Water Index (NDWI) in the delineation of open water features. *International Journal of Remote Sensing*, *17*(7), 1425-1432. doi:10.1080/01431169608948714

Meyer, F. (2019). Spaceborne Synthetic Aperture Radar – Principles, Data Access, and Basic Processing Techniques. *In SAR Handbook: Comprehensive Methodologies for Forest Monitoring and Biomass Estimation*. Eds. Flores, A., Herndon, K., Thapa, R., Cherrington, E. NASA. doi:10.25966/ez4f-mg98

Olthof, I., Fraser, R. H., & Schmitt, C. (2015). Landsat-based mapping of thermokarst lake dynamics on the Tuktoyaktuk Coastal Plain, Northwest Territories, Canada since 1985. *Remote Sensing of Environment, 168*, 194-204. doi:https://doi.org/10.1016/j.rse.2015.07.001

Park, H., Choi, J., Park, N., & Choi, S. (2017). Sharpening the VNIR and SWIR bands of Sentinel-2A imagery through modified selected and synthesized band schemes. *Remote Sensing*, *9*(10), 20. doi:10.3390/rs9101080

Planet Team (2017). Planet Application Program Interface: In Space for Life on Earth. San Francisco, CA. https://api.planet.com.

Pôssa, É. M., & Maillard, P. (2018). Precise delineation of small water bodies from Sentinel-1 data using support vector machine classification. *Canadian Journal of Remote Sensing*, *44*(3), 179-190. doi:10.1080/07038992.2018.1478723

Raynolds, M., Magnússon, B., Metúsalemsson, S., & Magnússon, S. H. (2015). Warming, sheep and volcanoes: land cover changes in Iceland evident in satellite NDVI trends. *Remote Sensing, 7*(8). doi:10.3390/rs70809492

Robertson, W., Zhang, K., & Whitman, D. (2007). Hurricane-induced beach change derived from airborne laser measurements near Panama City, Florida. *Marine Geology, 237*, 191-205. doi:10.1016/j.margeo.2006.11.003

Robinson, T.R. and Davies, T.R.H. (2013) 'Review article : Potential geomorphic consequences of a future great (Mw = 8.0+) Alpine Fault earthquake, South Island, New Zealand.', *Natural hazards and earth system sciences, 13*(9). pp. 2279-2299

Rokni, K., Ahmad, A., Selamat, A., & Hazini, S. (2014). Water feature extraction and change detection using multitemporal Landsat imagery. *Remote Sensing, 6*(5). doi:10.3390/rs6054173

Ryabchuk, D., Spiridonov, M., Zhamoida, V., Nesterova, E., & Sergeev, A. (2012). Long term and short term coastal line changes of the Eastern Gulf of Finland. Problems of coastal erosion. *Journal of Coastal Conservation, 16*(3), 233-242. doi:10.1007/s11852-010-0105-4

Singh, A. (1989). Review Article Digital change detection techniques using remotely-sensed data. *International Journal of Remote Sensing, 10*(6), 989-1003.

Sun, W., Chen, B., & Messinger, D.W. (2014). Nearest Neighbor Diffusion Based Pan Sharpening Algorithm for Spectral Images. *Optical Engineering 53*(1).

Sun, W. W., Du, B., & Xiong, S. L. (2017). Quantifying sub-pixel surface water coverage in urban environments using low-albedo fraction from Landsat imagery. *Remote Sensing*, *9*(5), 15. doi:10.3390/rs9050428

Torres, R., Mouginis-Mark, P., Self, S., Garbeil, H., Kallianpur, K., & Quiambao, R. (2004). Monitoring the evolution of the Pasig–Potrero alluvial fan, Pinatubo Volcano, using a decade of remote sensing data. *Journal of Volcanology and Geothermal Research, 138*(3), 371-392. doi:https://doi.org/10.1016/j.jvolgeores.2004.08.005

Wahab, L. and S. Sutomo (2019). Changes in vegetation on Mount Agung Volcano, Bali, Indonesia. *Journal of Tropical Biodiversity and Biotechnology, 4*.

Xu, H. (2006). Modification of Normalized Difference Water Index (NDWI) to enhance open water features in remotely sensed imagery (Vol. 27).

APPENDIX

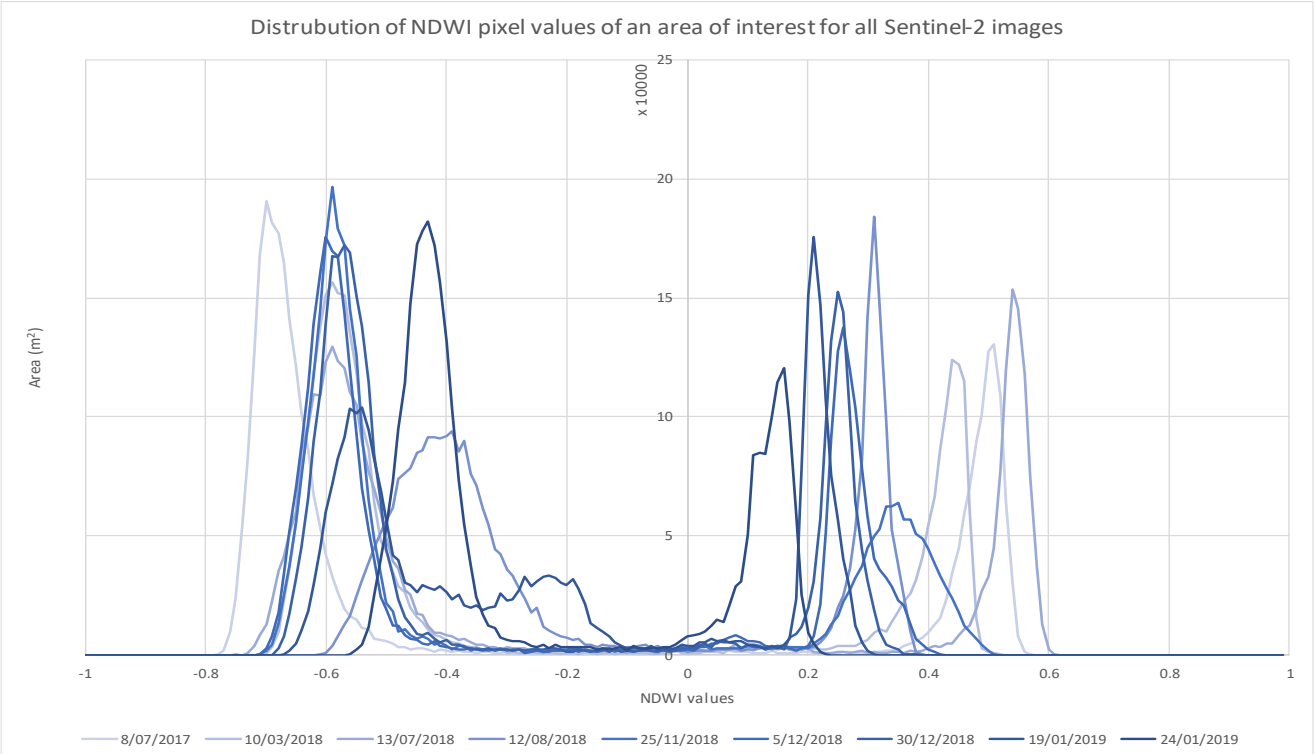

FIGURE 18 THIS GRAPH SHOWS THE DISTRIBUTION OF THE PIXEL VALUES FOR EACH INDIVIDUAL SENTINEL-2 NDWI IMAGE (E.G. FOR EACH IMAGE DATE). THE DATA EXTRACTED FROM THE IMAGES TO CREATE THIS GRAPH WAS FROM A SMALL AREA OF INTEREST RATHER THAN THE WHOLE SUBSET SO THAT ALL IMAGES WERE THE SAME SIZE AND CONTAINED NO CLOUD COVER.

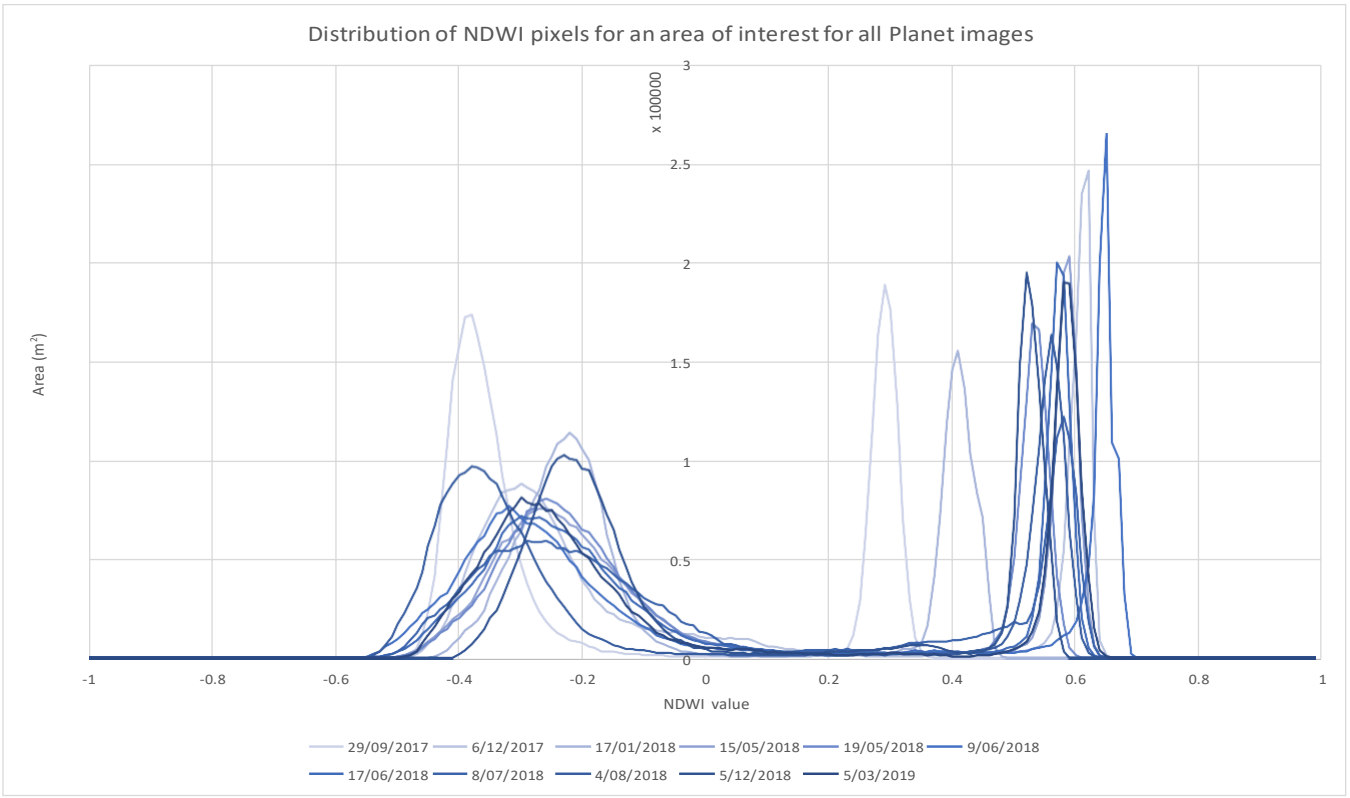

FIGURE 19 THIS GRAPH SHOWS THE DISTRIBUTION OF THE PIXEL VALUES FOR EACH INDIVIDUAL PLANET NDWI IMAGE (E.G. FOR EACH IMAGE DATE). THE DATA EXTRACTED FROM THE IMAGES TO CREATE THIS GRAPH WAS FROM A SMALL AREA OF INTEREST RATHER THAN THE WHOLE SUBSET SO THAT ALL IMAGES WERE THE SAME SIZE AND CONTAINED NO CLOUD COVER.

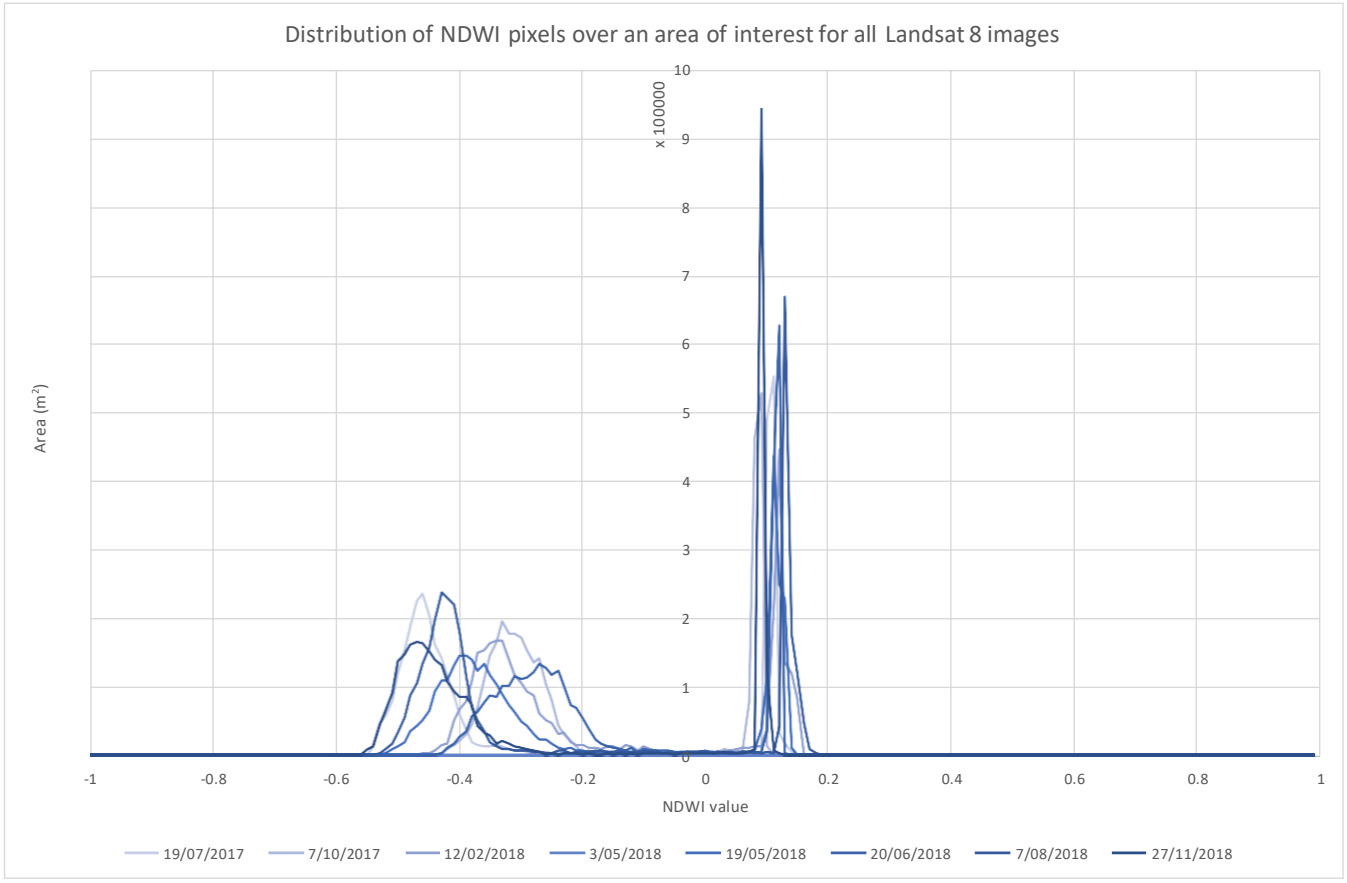

FIGURE 20 THIS GRAPH SHOWS THE DISTRIBUTION OF THE PIXEL VALUES FOR EACH INDIVIDUAL LANDSAT 8 NDWI IMAGE (E.G. FOR EACH IMAGE DATE). THE DATA EXTRACTED FROM THE IMAGES TO CREATE THIS GRAPH WAS FROM A SMALL AREA OF INTEREST RATHER THAN THE WHOLE SUBSET SO THAT ALL IMAGES WERE THE SAME SIZE AND CONTAINED NO CLOUD COVER.